Isotope Constraints on Paleo-Depositional Environments and Intra-Basin Correlation in the Proterozoic McArthur Basin, Northern Territory, Australia

Thesis submitted in accordance with the requirements of the University of Adelaide for an Honours Degree in Geology

William Casey Giuliano

November 2016

THE UNIVERSITY of ADELAIDE

TITLE

Isotope Constraints on Paleo-Depositional Environments and Intra-Basin Correlation in the Proterozoic McArthur Basin, Northern Territory, Australia

RUNNING TITLE

Isotope Constraints on Depositional Environments in the McArthur Basin

ABSTRACT

The Proterozoic McArthur Basin, Northern Territory, Australia, hosts some of the oldest proven hydrocarbon sources in the world including the organic rich black shale unit in the McArthur Group, the Barney Creek Formation. Stratigraphically positioned between dolomitic carbonate units, the depositional setting for the Barney Creek Formation has been in debate for at least three decades. Published literature supports both an anoxic coastal lagoon/lacustrine environment and also a relatively deep-marine low-energy deposition. Here we employ high-resolution records of stable isotope ratios ($\delta^{13}C$, $\delta^{18}O$ $^{87}Sr/^{86}Sr$) and elemental concentrations (Ba/Ca) in the carbonates rich sedimentary record of the McArthur Group (cores LV09001, McA5, Bj2, BCF 4) as proxies to constrain paleo-depositional environments. Using samples from the LV09001 core, we were able to create a high-resolution, geochemical and isotope ratio profile of the Glyde Package, McArthur Group. Ranging from the Emmerugga Dolomite to the Donnegan Member. Acquired $\delta^{13}C$, $^{87}Sr/^{86}Sr$ and Ba/Ca stratigraphic trends indicate a changing paleo-environment at the time of sediment deposition and carbonate precipitation. In particular a systematic negative $\delta^{13}C$ anomaly, magnitude around 2.5‰, is recorded in the Barney Creek Formation, where Ba/Ca ratios are also anomalously high and coeval $^{87}Sr/^{86}Sr$ trend indicates a 'non-marine' restricted environment. Observed light carbon (^{12}C), and elevated barium concentrations (Ba/Ca ratios) are likely controlled by local cycling of organic matter in a redox-stratified restricted basin analogous to modern Black Sea. A restricted setting also aids in chemical and redox stratification, creating deep water anoxic and low energy conditions for the deposition of the Barney Creek Formation. Finally, our constraints from coupled C and Sr isotope data, collected from the most 'marine' carbonate intervals, suggest that the inferred $\delta^{13}C$ and $^{87}Sr/^{86}Sr$ signatures of Proterozoic paleo-seawater (at about 1640 Ma) were close to -0.5 to 0 per mil, and 0.705 to 0.706, respectively.

KEYWORDS

Isotopes, Carbon, strontium, Oxygen, Carbonates, McArthur Basin, Depositional Environment, Proterozoic

TABLE OF CONTENTS

LIST OF FIGURES AND TABLES

INTRODUCTION

The McArthur Basin is a large intracratonic sedimentary basin covering an area of around 180,000 km^2 in northern Australia. It is comprised of thick Paleoproterozoic and Mesoproterozoic successions, subdivided into a number of sedimentary packages. Source rocks with some of the world's oldest hydrocarbon deposits occur mostly in the youngest (ca. 1490 to 1325 Ma) dominantly siliciclastic sedimentary Wilton Package which hosts the organic-rich Kyalla and Velkerri Formations. These source rocks have experienced a relatively low degree of post-depositional alteration and thus contain prospective Proterozoic hydrocarbon resources. The stratigraphically older packages (i.e., Glyde Package ca. 1640 to 1600 Ma) also contain hydrocarbon deposits (Kelly et al. 2010). The Glyde Package comprises of the Barney Creek Formation and numerous occurrences of sedimentary carbonate sequences, dominated by *platform dolostones* from various shallow-marine to coastal and continental 'sabkha-playa' depositional settings.

The paleo-depositional environments of these carbonate sequences and associated hydrocarbon deposits in the McArthur Basin have been a matter of debate for three decades. Available studies provide conflicting interpretations. Earlier work and lithological descriptions suggest a lacustrine environment for carbonate deposition (Logan and Williams 1984, Jackson et al. 1987). More recent studies favour a shallow to moderately deep marine environment similar to a modern Black Sea style setting, with a redox stratified water column comprising of oxic to euxinic basinal marine settings (Jackson and Southgate 2000, Lindsay and Brasier 2000, Shen et al. 2002). The redox conditions and stratification are necessary for the explanation of an organic-rich, shale member in the Barney Creek Formation of the Glyde Package, and the base metal mineralisation in the coeval dolomitic shales for the world-class stratiform Zn-Pb-Ag ore deposits of the McArthur River Mine. The plausible water depths and relative sea level changes during the deposition of the Barney Creek Formation are also disputed (Davidson and

Dashlooty 1993, Bull 1998b). Semi-restricted, epicontinental seas such as the modern day Black Sea and the McArthur basin lack water mixing. Physical and chemical stratification of local water masses in these settings can occur due to salinity and temperature gradients. Freshwater reaching the basin is less dense than typical seawater, and therefore floats on the existing saline water causing an efficient physical separation of the shallow versus deep waters. A thermohaline stratification in turn, can lead to a redox stratification of the basin. The surface layer of shallow waters being in the photic zone and in contact with atmospheric oxygen allows for microorganisms to photosynthesise creating oxygenated conditions at shallow depths. In contrast, the deeper waters are devoid of free oxygen (O_2) and are enriched in sulphide anions (S^{2-}), causing deep-water anoxic conditions and redox stratification.

Recent geochemical and isotope studies on the Black Sea and other anoxic water bodies show a systematic variation in the ratio of stable isotopes of carbon (^{13}C to ^{12}C ratio) with water depth. Deeper waters are enriched in lighter carbon isotopes due to the decay and remineralization of ^{12}C rich organic matter present within the sediments (Fry et al. 1991, van Breugel et al. 2005). Other proxies sensitive to the production and decay of organic matter, such as elemental Ba/Ca ratios, also show a systematic variation with water depth in the Black Sea (Falkner et al., 1993). Deep, bottom waters have elevated Ba concentrations due to the input of organically-complex Ba from organic matter. Thus, if the Proterozoic depositional environment within the McArthur Basin was indeed analogous with a modern Black Sea having a redox stratification. One would expect to observe consistent geochemical and isotope patterns in the studied Proterozoic sedimentary record (assuming that the redox conditions in the McArthur Basin and/or the depth of sediment deposition fluctuated over time). One of the goals of this project is to employ selected elemental and isotope proxies (i.e., carbon, oxygen and strontium isotopes, as well as elemental/calcium ratios) for the further constraint on temporal changes in the paleo-depositional environment during the deposition of the Barney Creek

Formation and the associated carbonate/dolomite sequences. Deposited carbonate rocks preserve the carbon isotopic ratio ($\delta^{13}C$) of the ambient dissolved inorganic carbon (DIC) in the seawater and/or basinal fluids, and thus reflects past environmental conditions and changes in the marine carbon cycle through time. The Proterozoic marine $\delta^{13}C$ record is well constrained, based on the analysis of marine carbonate rocks, and these data revealed several significant $\delta^{13}C$ excursions associated with major tectonic and climatic events in geological time (Shields and Veizer 2002).

As to other isotope tracers, studies on Proterozoic carbonates from different locations and paleo-continents have shown a systematic correlation of strontium isotopes ($^{87}Sr/^{86}Sr$) with changing deposition environment, such as open marine to coastal sabkha-playa settings (Melezhik et al. 2005, Kuznetsov et al. 2010). Importantly the radiogenic $^{87}Sr/^{86}Sr$ proxy in preserved sedimentary carbonates can be used to determine past depositional changes in the continental runoff and riverine Sr fluxes into the basin through time (Shields and Veizer 2002). Therefore, a multiproxy isotope approach based on $^{87}Sr/^{86}Sr$ and $\delta^{13}C$ tracers provide information on past depositional environments and thus differentiate between *open marine* against more *restricted* and continentally influenced settings. Specifically, dolostones from supratidal (playa) settings tend to yield heavier $\delta^{13}C$, and more radiogenic $^{87}Sr/^{86}Sr$ signatures compared to samples deposited in more marine and/or intertidal (sabkha) settings (Melezhik et al. 2005, Kuznetsov et al. 2010, Farkas. J. 2013). As to elemental proxies, such as barium, oceans generally have a low level of dissolved barium in the surface waters comparative to deeper water. The depleted levels of barium in shallow depths can be attributed to biogenically mediated barite ($BaSO_4$) formation in the surface waters. Higher concentrations at depth are due to an input of barium from decaying organic matter in deep-sea sediments.

The geochemical techniques and isotope proxies outlined above ($\delta^{13}C$, $\delta^{18}O$, $^{87}Sr/^{86}Sr$, and elemental/Ca ratios) will be used in this study to reconstruct paleo-environmental conditions

as well as depositional settings (marine vs. restricted) in the McArthur Basin based upon sedimentary records dated at about 1600 to 1640Ma. In addition, comparing geochemical trends and isotope data from coeval and correlative sedimentary records sampled across the basin (i.e., drill cores LV09001, McA5, Bj2 and BCF SC 4, see Figure **1**). This project will also aim to use the generated results for an isotope chemostratigraphy and intra-basin correlation. Apart from the relevance for applied research and industry, i.e., hydrocarbon exploration, this project also has significance for basic research and earth system evolution studies. The generated isotope trends shed more light on the chemical and isotope composition of the Paleo to Mesoproterozoic seawater, and coeval climatic and tectonic changes occurring during this geological interval.

For this study we selected the LV09001 drill core as a 'reference' for the McArthur Group, and thus this core was sampled at relatively high-resolution. The generated elemental and isotope trends were used as 'reference curves' for our intra-basin correlation based on data acquired from other cores. The LV09001 core has been chosen as it is freshly cut, well persevered and has extensive coverage of the McArthur Group. It was also recently studied and described in detail regarding lithological and mineralogical changes (Schmid 2015). In addition, the LV09001 core provides an almost complete and continuous record of the key formations in the McArthur Group, including the Barney Creek Formation, and the underlying and overlying dolomite formations, such as Emmeruga, Teena, Cooley and Reward Dolomites.

Regional Geological Setting

The McArthur Basin is a vast intracratonic sedimentary basin underlying a large proportion of the north-eastern Northern Territory (Figure 1). The thick Paleoproterozoic and Mesoproterozoic packages are relatively undeformed and have been subdivided into a number

of different sedimentary packages (Ahmad and Dunster 2013). The Glyde Package in the Batten Fault Zone contains a significant volume of sedimentary carbonates, mainly platform stromatolitic dolostones (e.g. the McArthur and Vizard Group) formed presumably in coastal sabkha-playa and shallow marine depositional environments. Proven source rocks in the Glyde package have experienced a relatively low degree of post-depositional alteration and contain prospective Proterozoic hydrocarbon resources. Sedimentary packages distributed across northern Australia show many similarities in stratigraphic sequence to the McArthur Group (Page and Sweet 1998).

Previous studies on the Glyde Package have constrained the age of The Barney Creek Formation to be around 1640 ± 3 Ma (Page et al. 2000). Paleo-tectonic reconstructions and models for this time period suggest the McArthur Basin formed as an inland sea (Betts et al. 2016), west of the modern day Gulf of Carpentaria (Figure 1). The shallow to deep water paleo-environments allowed for an extensive carbonate platform to form gradually.

Based on the lithological descriptions, sedimentary features, and mineralogical data (acquired from HyLogger^{TM}) from the selected drill cores, the proposed changes in the depositional environment for the McArthur Group have been controlled by sea level changes and subsidence in a rifting basin (Schmid 2015)(Figure 2).

The oldest formation sampled in this study is the Emmerugga Dolomite which is believed to have been deposited in a relatively shallow open marine to lagoonal setting (Figure 3a). The overlying Teena Dolomite member indicates further shallowing of the basin, based on evaporite mineral pseudomorphs as well as karst features (Figure 3a) see also (Schmid 2015). Brecciated debris flows of Teena and Emmerugga Dolostones clasts in the overlying Cooley Member indicate a sea level fall and shelf exposure (Figure 3b).

The Barney Creek Formation deposited above the Cooley Member is predominately composed of a dark, carbonaceous, and thinly bedded organic-rich mudstone. Pyrite mineralisation is

present through the lithology with occasional massive brecciated sections similar to the Cooley Member. Uplift and resulting subsidence due to rifting, created the accommodation space required for this low energy anoxic deposition in presumably redox stratified marine to lagoonal settings. (Figure 3b). The gradational contact with the overlying Reward Dolomite resembles the lower lithologies with karst features and occasional brecciated sections. Finally, the Hot Springs Member is a stromatolitic and highly silicified dolostone with interbedding of silicified evaporite minerals, and the Donnegan Member is a grey/green dolomitic siltstone with sandy layers towards the top signifying a deposition close to the shoreline (Figure 3c)(Schmid 2015).

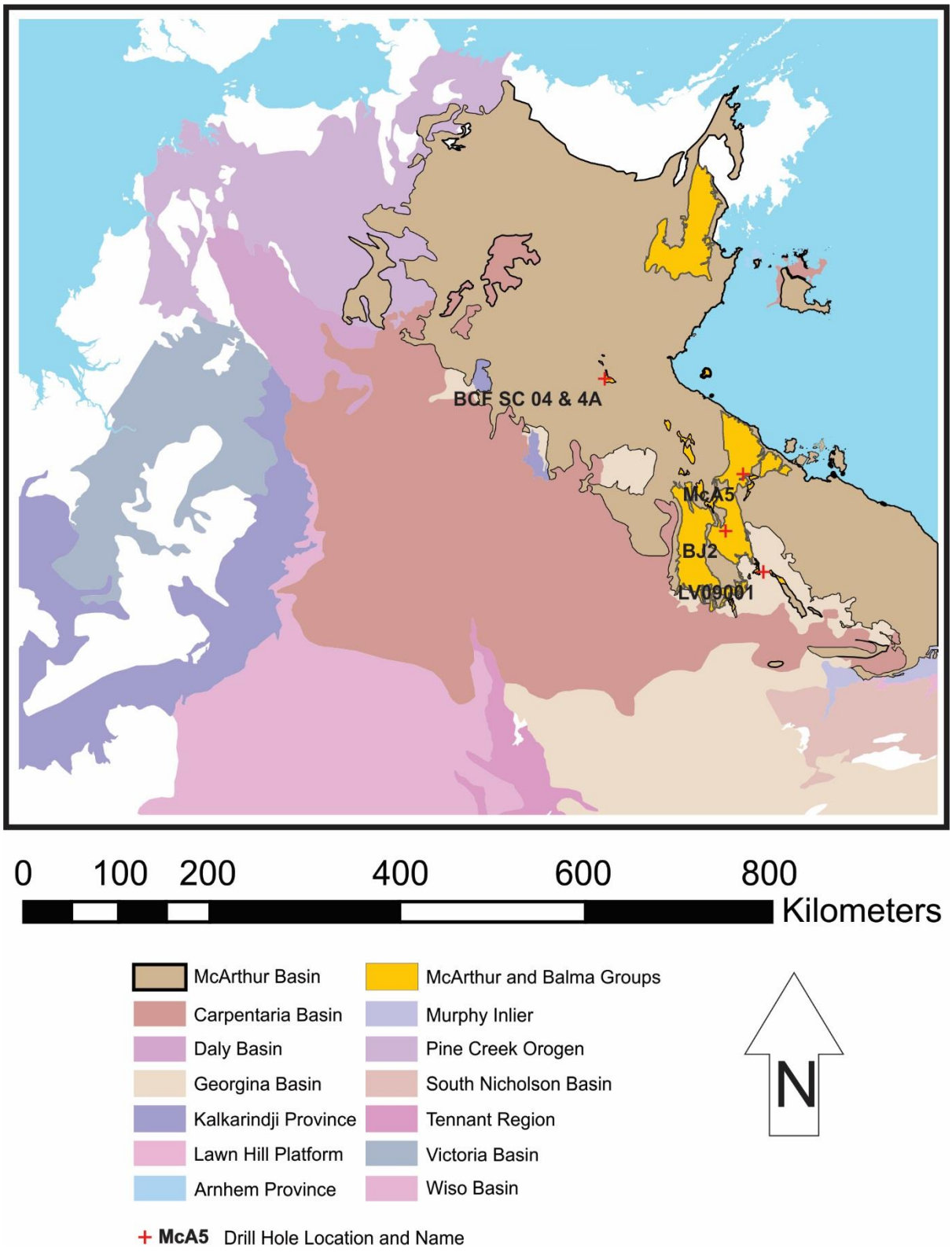

Figure 1. A map of the modern-day location of the McArthur Basin (brown) with selected drill cores which intersect the Glyde Package in the McArthur Group. LV09001 is the main focus of this study due to its extensive coverage and well-described lithology with HyLoggerTM Data (Schmid 2015). Adapted from NTGS STRIKE data.

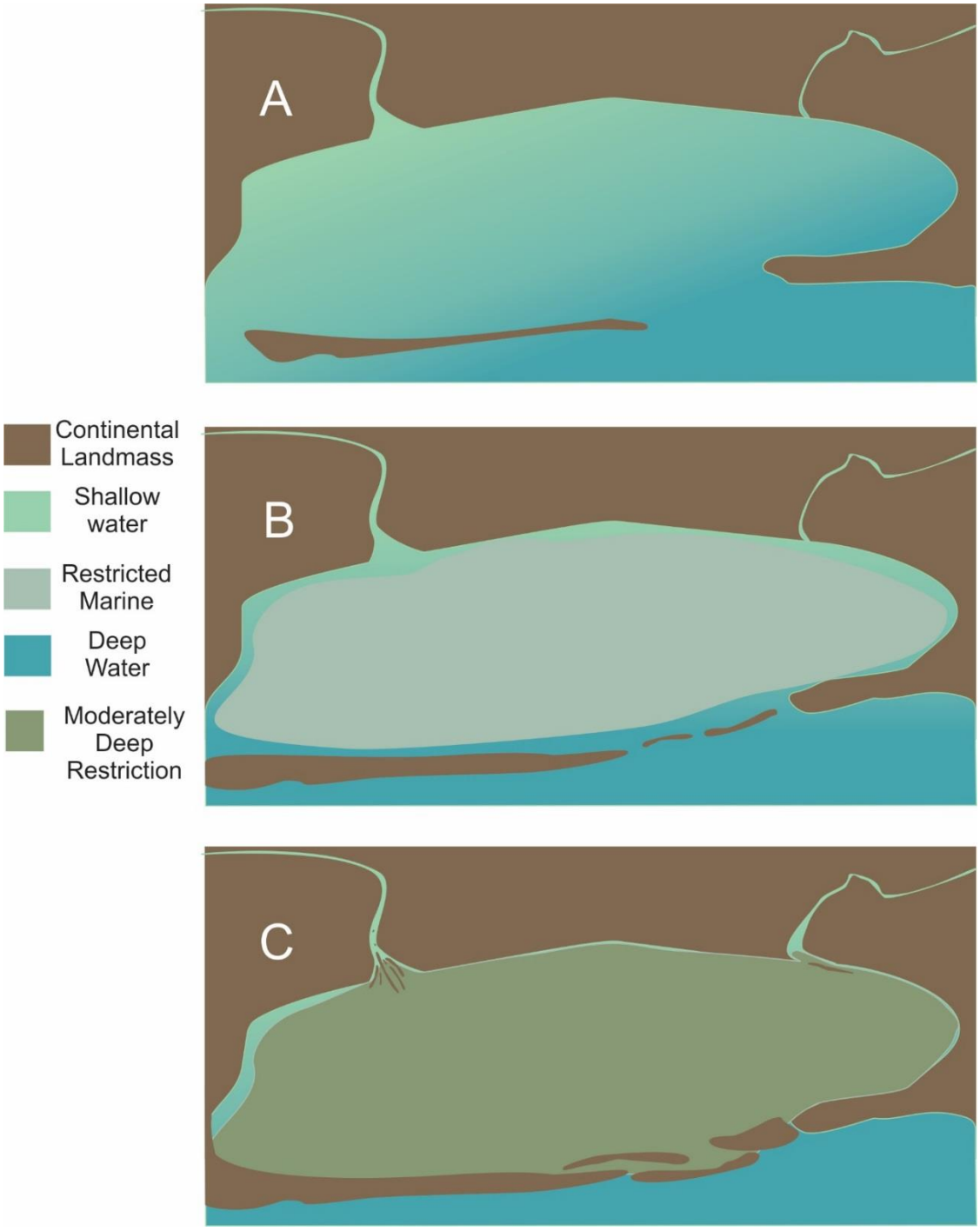

Figure 2. The inferred restriction of the McArthur Basin from above demonstrating the sea level change and lack of ocean water input. The change in source alters the water chemistry and in turn alters the sediments deposited. A) Shallow open marine setting where the basin is well connected to the open ocean allowing for water mixing within the basin. The majority of water input originates from the ocean with slight input from continental rivers. B) Regressive sea level, the semi-restricted basin is no longer well connect to the ocean due to the falling sea level. Stratification of the basin due to density difference of fresh and saline water. Limited water input from the ocean with increased input from continental rivers. C) Restricted marine basin has extremely limited input from ocean water; the majority is from continental runoff. Stratification causes anoxic conditions (similar to the Black Sea). Gentle rift-related subsidence in the basin, allows for deposition of organic-rich BCF shale member preserved under the anoxic conditions.

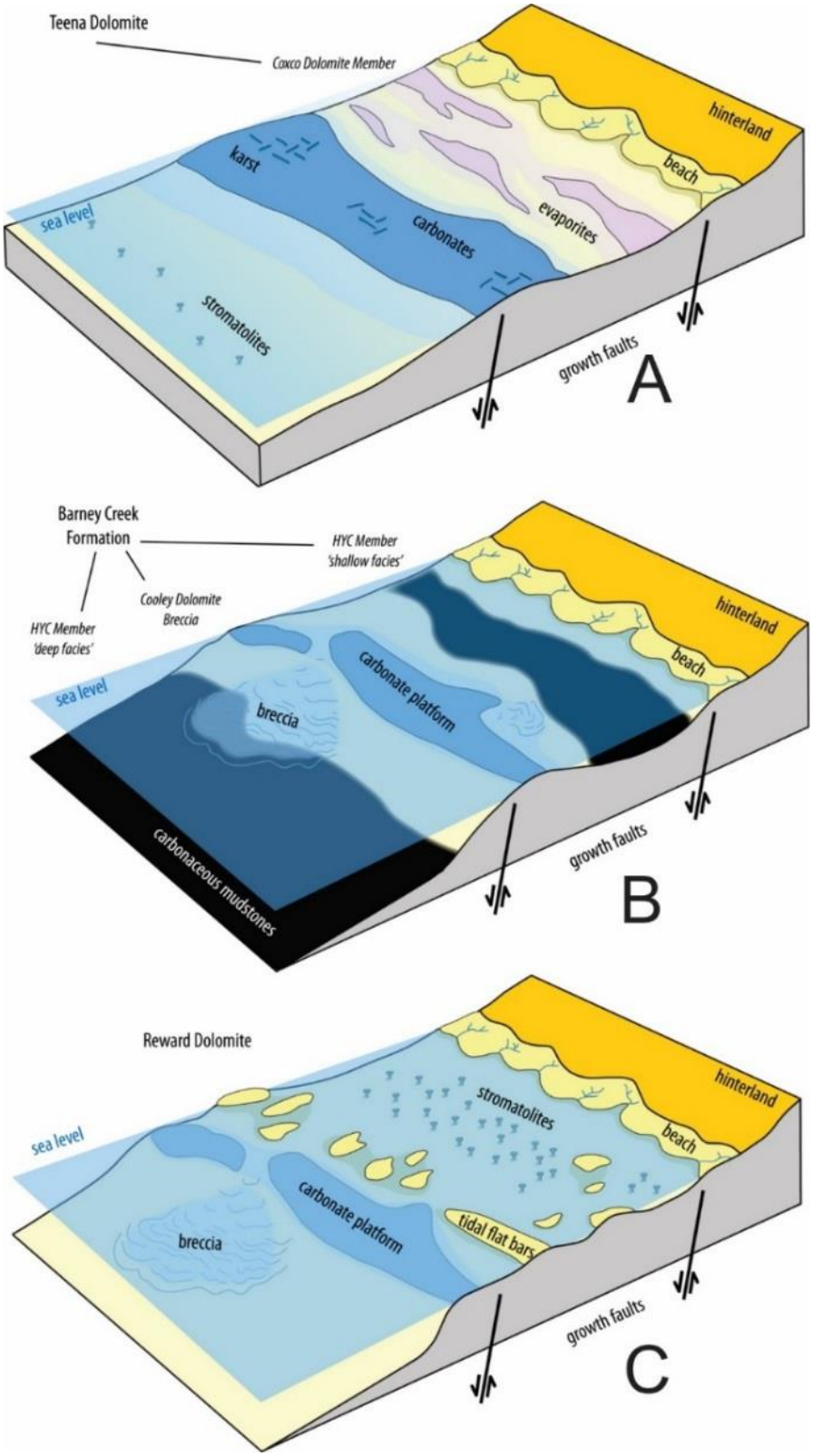

Figure 3. A reconstruction of the paleo-depositional environment based on lithological observations of sedimentary features and minerology, based on (Schmid 2015). The main characteristic lithologies of LV09001 have been roughly constrained to these different depositional environments. A) shows a shallow marine setting and the environments that allowed for a carbonate shelf to form. B) shows the restricted settings with redox stratified structure of the basin that allowed the deposition of organic rich shale within the Barney Creek Formation in the low energy and anoxic settings. C) is the relatively shallow marine to lagoonal setting close to the shoreline.

METHODS

Sampling of drill cores

The studied drill cores (LV09001, McA5, Bj2 and BCF SC 4) were strategically selected based on their location, stratigraphy, and lithology, with the aim to sample predominantly relatively carbonate-rich sequences intersecting the McArthur Group. Using the data from the HyLogger™ (Hyperspectral Logging) instrument at NTGS (Northern Territory Geological Survey), and the spectral geologist software to view HyLogger™ data packages (TSG™ Viewer software). We determined the depths from which the samples for this project will be taken from (based primarily on carbonate/dolomite contents of these rocks), with the aim to sample the most carbonate-rich sediments from the drill cores. In general, the samples were taken every 5 to 10 m depending on the carbonate contents and the representative lithology at that particular depths. Selected samples were then cut into quarter sections using an automated rock saw at the NTGS core facility in Darwin. For the 'reference' core LV09001 we selected 57 samples, where other cores used in this study were sampled more sporadically (McA5 = 14 samples, Bj2 = 12 samples, BCF 4 = 10 samples and BCF 4a = 7 samples).

Preparation of thin sections

A total of 18 different samples, with main representative lithologies, were selected from the quarter cores throughout the LV09001 core, to be cut and prepared for standard 46mm x 26mm (30 microns in thickness) polished thin-sections. Optical petrography was completed on an Olympus BH-2 optical microscope and XRF elemental mapping was conducted on the slides using the Quanta 600 SEM and EDAX Genesis to do EDS mapping. The Quanta 600 SEM was calibrated to a gold standard and focused at 10mm away from the slide. Photomicrographs are shown in the Appendix.

Determinations of carbonate contents, and stable carbon ($\delta^{13}C$) and oxygen ($\delta^{18}O$) isotope compositions

The analysis of $\delta^{13}C$ and $\delta^{18}O$ values in carbonates, and the percentage (wt%) of dolomite in the bulk rocks, involved the micro-drilling on homogenous areas representative of each sample using a diamond dentistry drill. Approximately 300 mg of powder was drilled from each sample onto a piece of weight paper, which was then transferred to a plastic micro-centrifuge tube. To calculate percentage dolomite, each powder sample had to be precisely weighed to around 0.5 - 2.0 mg before being placed into 1 ml glass septa-vials. Values were obtained using Isotope Ratio Mass Spectrometry (IRMS) at the University of Adelaide's Fisons Optima isotope ratio mass spectrometer, dual inlet IRMS combined with Fisons Isocarb Carbonate Preparation System. Carbon and oxygen isotope ratios were recorded in conventional delta notation (see below) with respect to PDB (Pee Dee Belemnite). An in-house standard ANU-P3 (Australian National University- carbonate) was used during the actual isotope analysis. The analytical errors (2SD) for $\delta^{13}C$ and $\delta^{18}O$ values are on the order of 0.05 per mil (‰) or better.

The carbon isotope compositions presented in this study are expressed in delta notation ($\delta^{13}C$), in per mil (‰), normalised to PDB (or VPDP) standard, using the following equation:

$$\delta^{13}C\ (‰) = [(^{13}C/^{12}C_{SAMPLE}) / (^{13}C/^{12}C_{STANDARD}) - 1] \times 1000$$

Similarly, the oxygen isotope compositions are also expressed as delta notation ($\delta^{18}O$), in per mil (‰), normalised to PDB standard, based on the following equation:

$$\delta^{18}O\ (‰) = [(^{18}O/^{16}O_{SAMPLE}) / (^{18}O/^{16}O_{STANDARD}) - 1] \times 1000$$

Determination of strontium isotope composition ($^{87}Sr/^{86}Sr$ ratios)

Prior to Sr isotope analyses, the strontium fractions have to be purified from the sample matrix, and this step was achieved in a clean laboratory using a conventional strontium-specific resin Eichrom Sr-Spec in Teflon micro-columns using suprapure nitric acid (HNO_3) and water (H_2O) as working solutions. The purified Sr fractions (ca. 1000 nanograms of Sr) were then used for the subsequent isotope analysis of $^{87}Sr/^{86}Sr$ ratios.

High precision measurements of $^{87}Sr/^{86}Sr$ in selected carbonates were done by the thermal ionisation mass spectrometry (TIMS), i.e., Phoenix TIMS instrument, with a reproducibility at two standard errors (2se) better than 0.000005, as determined by repeat measurements of standards and/or multiple replicates of individual samples. The Sr standard used for our TIMS measurements was SRM 987. For a detailed description of sample loading and filament ionisation, and reproducibility of the measured $^{87}Sr/^{86}Sr$ ratios, see Appendix.

Determination of elemental concentrations in bulk carbonate rocks

For elemental and strontium isotope analysis (see below), the rock powders from selected samples were reacted with supra pure 2N hydrochloric acid (i.e., distilled HCl) at room temperatures for 24 hours in Teflon vials, to leach mostly carbonate fraction of the rocks, thus avoiding the dissolution of siliciclastic components. This approach, adopted from (Melezhik et al. 2005, Kuznetsov et al. 2010), was used to minimise the contribution of non-marine (i.e., silicate) phases from the bulk sediment, with the aim to leach primarily, the ‘marine’ carbonate/dolomite phases. Thus reflecting the elemental and isotope compositions of the coeval seawater and/or local basinal waters from which the carbonates were formed.

Trace element concentrations of the samples were measured at Adelaide Microscopy, The University of Adelaide, using solution-based inductively coupled mass-spectrometry (ICP-MS). The analysis was done on an Agilent 7500ce (Agilent Technologies, Tokyo, Japan), equipped with an octopole collision system for the removal of polyatomic interferences. For sample introduction, the ICPMS was equipped with a Miramist nebuliser and a quartz spray chamber, into which samples were introduced by a peristaltic pump at a flow rate of 1.0mL/min. An internal standard, Indium, was mixed online with the samples to compensate for matrix effects. All element concentrations were determined against certified multi-element calibration standards (Choice Analytical, Australia) and blanks were interspersed throughout the analysis session, as well as measurement of the 200ppb calibration solution to check the instrument stability. The instrument was operated with an RF power of 1500W, a carrier gas flow of 0.89 L/min and a make-up gas flow of 0.19 L/min. Sample uptake rate was 1.0 mL/min and the dwell times ranged between 10ms to 1s. Three replicates were obtained for each sample. The data was processed using Agilent MassHunter Data AnalysisTM.

OBSERVATIONS AND RESULTS

Photomicrographs of thin sections—Optical and Elemental Maps

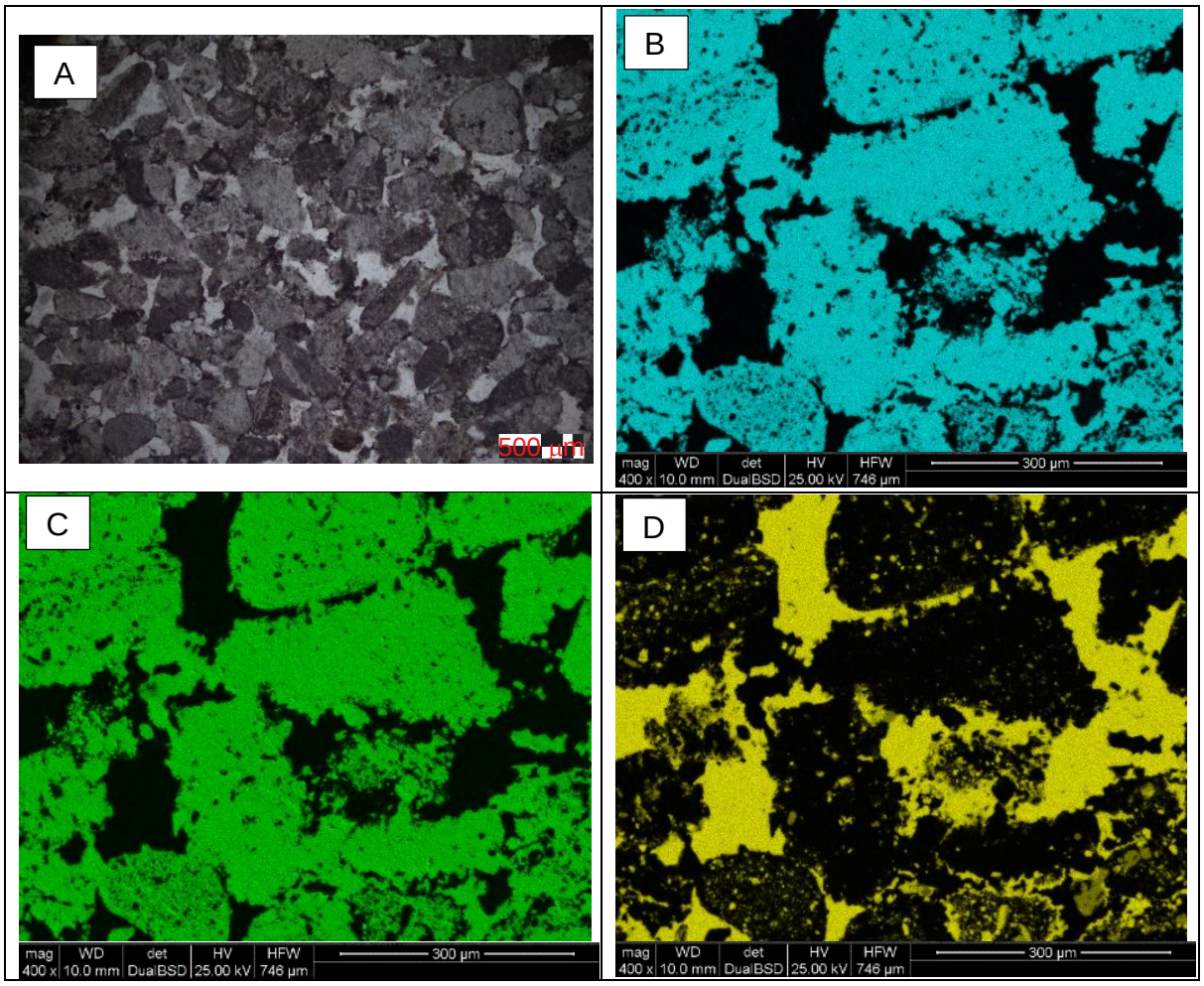

Figure 4. Microscope imagery from thin section sample LV5 from the Teena Dolomite. Sample LV 5 Teena Dolomite 568.28m

- **A) Transmitted light of thin section**
- **B) XRF element map of calcium**
- **C) XRF element map of magnesium**
- **D) XRF Map of silicon**

The Teena dolomite is made up of fine micritic to medium size grains 0.5mm dolomite clasts (Figure 4) with the occasional brecciated fragments. Small tuffaceous units and stromatolites are found in within the Teena Dolomites particularly near the top of the unit where the depositional environment is interpreted to be a shallow evaporitic setting. A silica-rich matrix hosts the grains which indicate a separate diagenesis event (i.e. infilling of pore space with Si-rich Fluids after the deposition of carbonate/dolomite clasts). The Teena Dolomite represents an ‘end-member’ situation of deposition where there is a dolomite-clast dominated lithology with a siliceous matrix.

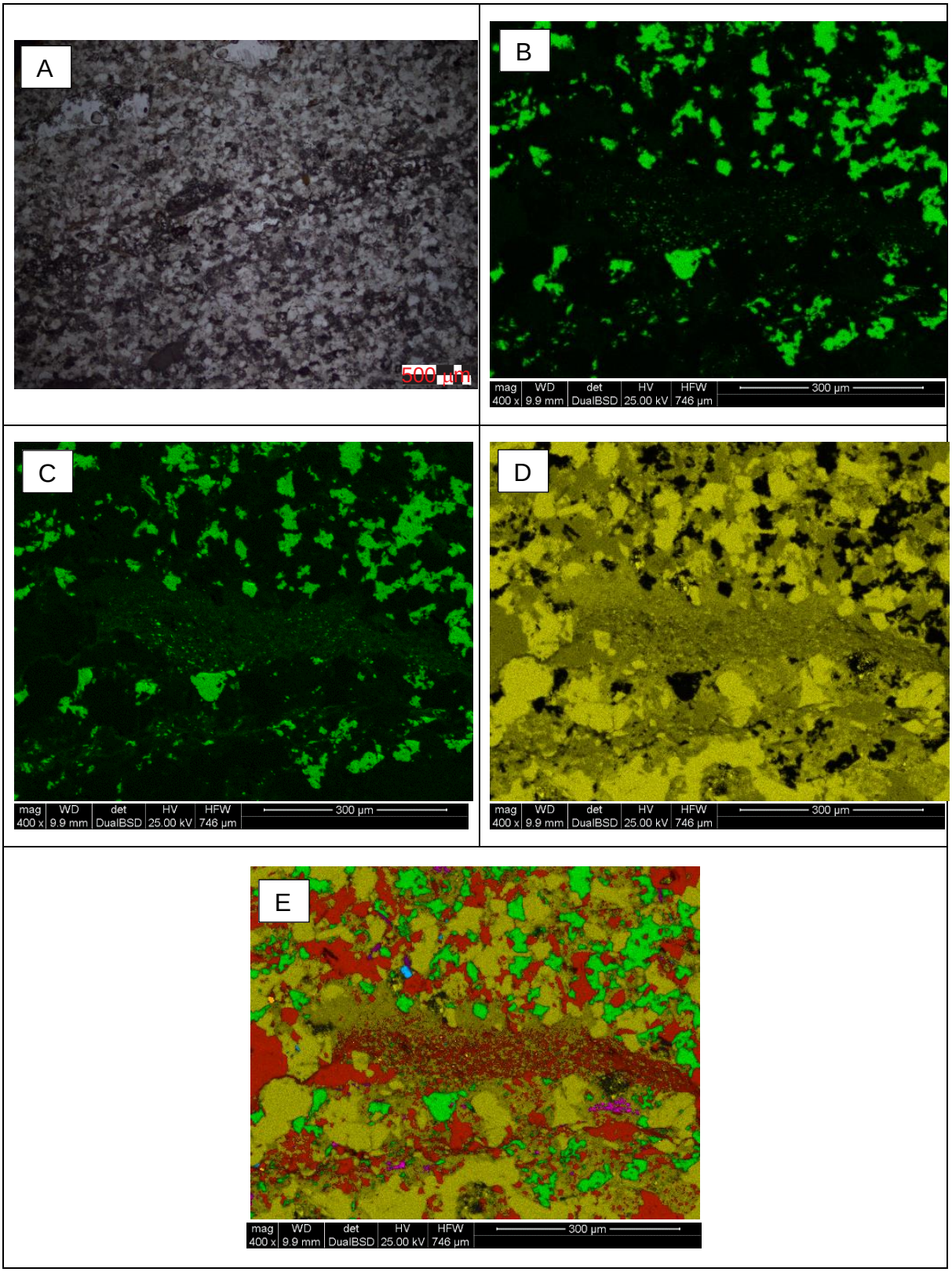

Figure 5. Microscope imagery from thin section sample LV44 from the Hot Springs Member 289.85m

- **A) Transmitted light of thin section**
- **B) XRF element map of calcium**
- **C) XRF element map of magnesium**
- **D) XRF Map of silicon**
- **E) Combined elemental XRF map demonstrating the angular carbonate grains conforming around the more rounded silicate clasts. The red infill highlights potassium in the sample portraying potassic alteration and fluid movement. Platinum and titanium grains are present in close**

proximity to the vein. Iron sulphide is also found proximal to the potassic fluid around the silica grains

The Hot Springs Member is an example of the intermediate style of deposition and diagenesis of carbonate seen in the lithology of LV09001. It is a silicified dolomite and finely laminated mudstone with occasional thin (< 0.5mm) organic-rich layers Due to the relatively close deposition to the shoreline there is an increase in fine silica clasts. The cement replacement seen in red in the XRF imagery of the sample is likely feldspar authogenisis from metal bearing (Ti, Fe, Pt) potassic fluid, post deposition.

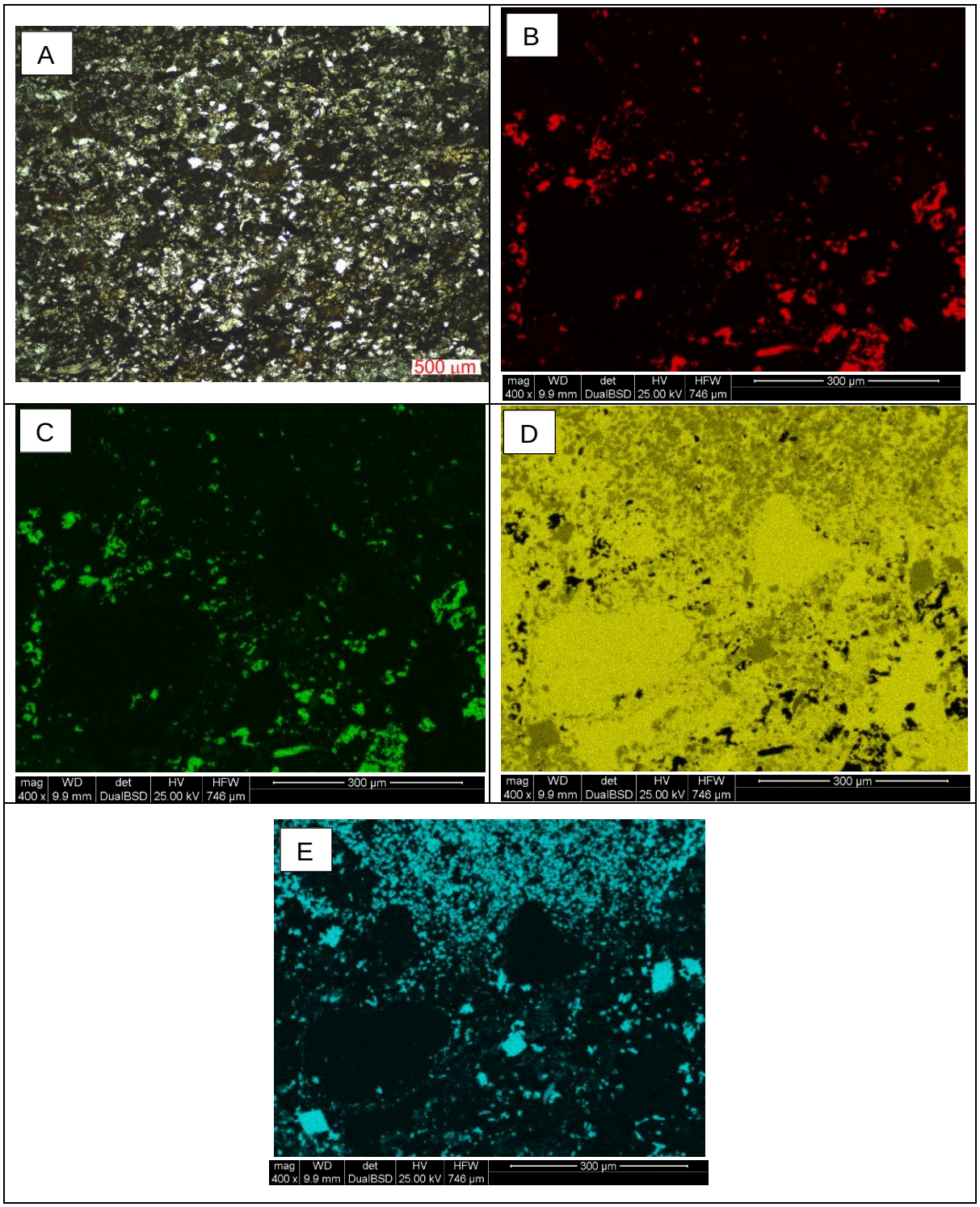

Figure 6. Microscope imagery from thin section sample LV37 from the Reward Dolomite 350.90m

- **A) Transmitted light of thin section**
- **B) XRF element map of calcium**
- **C) XRF element map of magnesium**
- **D) XRF element map of silicon**
- **E) XRF element map of potassium**

The Reward Dolomite hosts finely bedded siltstones with occasional tuffaceous layers, minor breccias and karst features. Samples from the Reward Dolomite shown in Figure 6 are highly silicified and show relatively large silica grains supported by a fine-grained carbonate-rich clay. Other sections contain spheroidal microfossil groupings. In an organic-rich matrix. The spheroids are roughly 10 μm in diameter likely from an ancient *Chroococcales* order of cyanobacteria (Oehler 1977) (Figure 7).

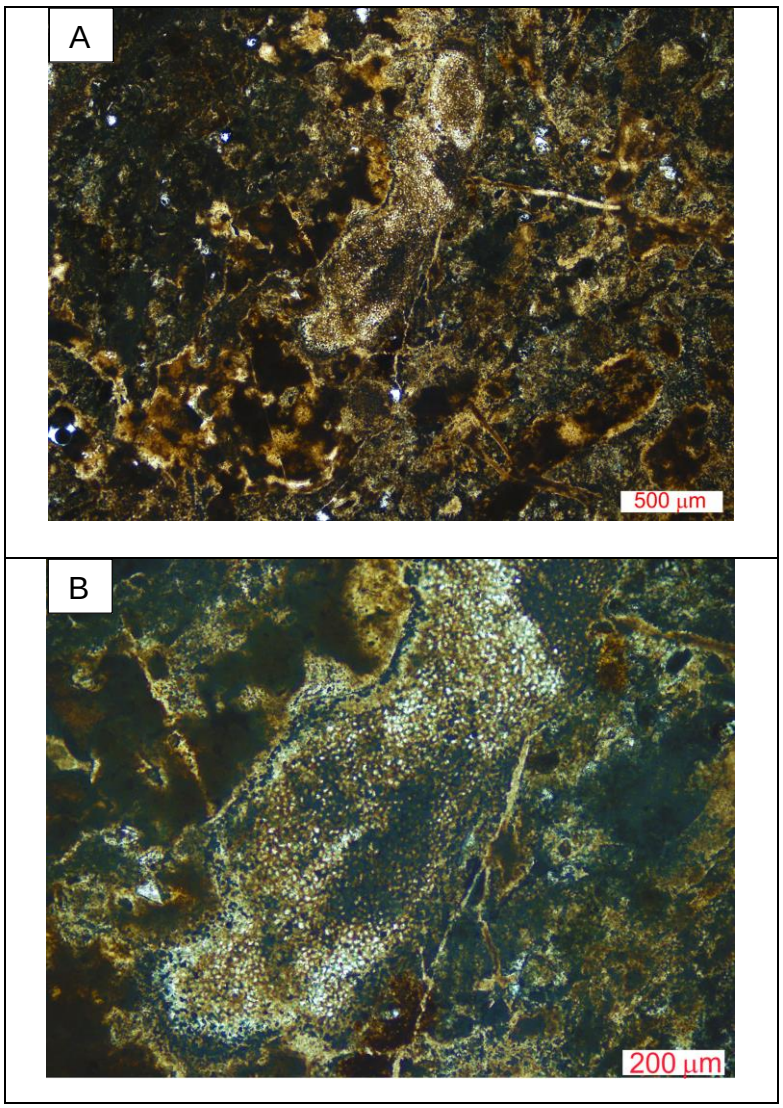

Figure 7. Thin section photography from sample LV37 in the Reward dolomite A is at 4x magnification and B is at 10x. The presence of coccoid microfossils has been preserved.

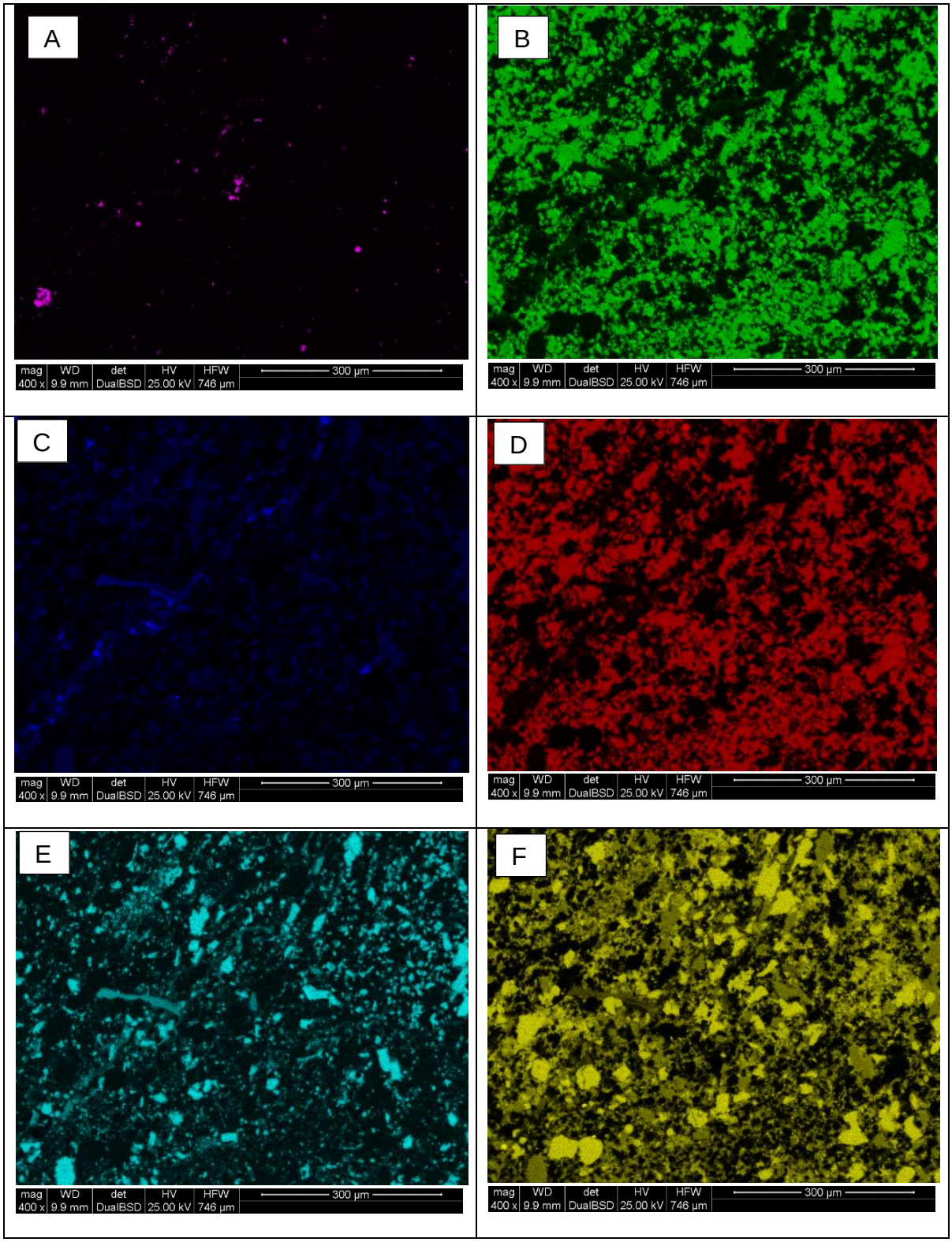

Figure 8. XRF elemental mapping of sample LV 30 from the Barney Creek Formation 393.70m

A) XRF image of sulphur
B) XRF image of magnesium
C) XRF image of aluminium
D) XRF image of calcium
E) XRF image of potassium
F) Map of silicon

Figure 8 demonstrates the low energy environment of the Barney Creek Formation. Observed are finely laminated, clay-rich layers, interbedded with a dolomite cement and silicate clasts. The depth of deposition of the Barney Creek Formation is debated as the sedimentary features suggest a low energy deep marine style setting with high concentrations of organic matter. High quantities of iron sulphides are found throughout the Barney Creek Formation, an indication of anoxic bottom waters during deposition (Figure 8c) (Boesen and Postma 1988, Shen et al. 2003)

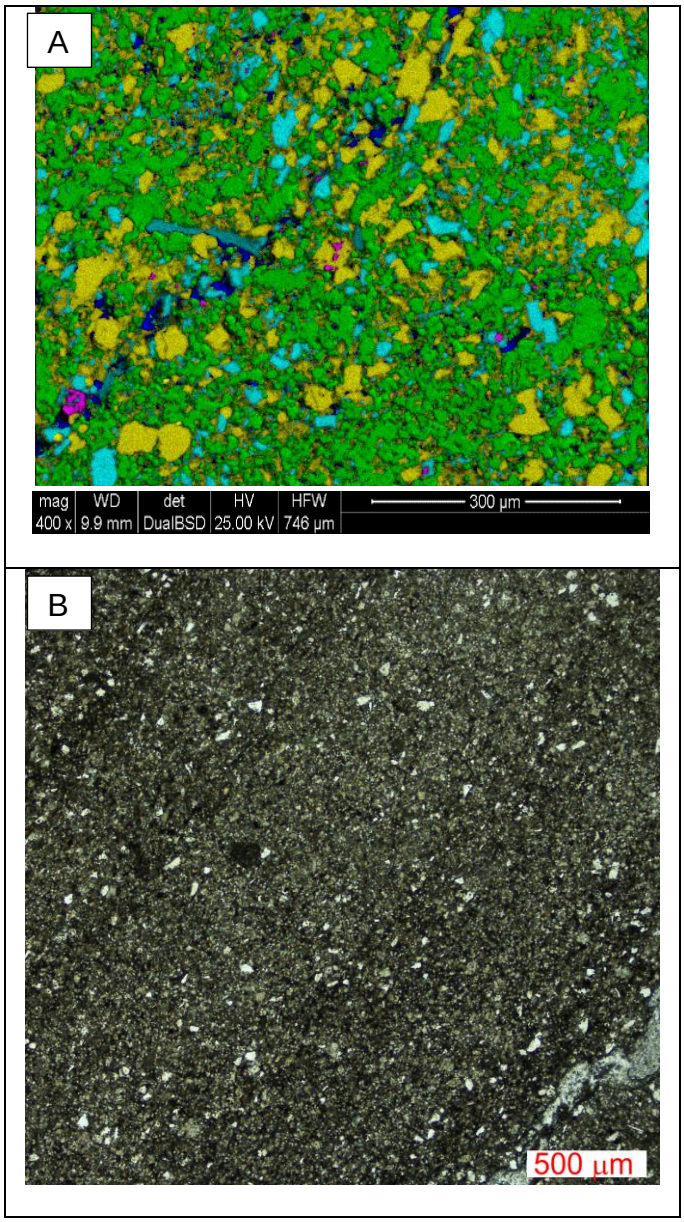

Figure 9. A) is a combined XRF elemental map of sample LV30 showing the interactions of silicon, aluminium, carbonate (combined Ca and Mg), sulphides (combined S and Fe), and potassium. B) 4x magnification of the Barney Creek Formation from sample LV 30.

Stratigraphic trend of $\delta^{13}C$ through LV09001

High-resolution carbon isotope data were taken from LV09001 sampled every few metres through the core with a focus on getting a general representation of the δ13C trend with stratigraphic depth (Figure 10). In stratified anoxic water body such as the Black Sea, the δ13C values of the DIC in the water column vary with depth (Fry et al. 1991). Accordingly, the δ13C values of carbonates deposited in an anoxic stratified basin can be an indicator of the relative depth at which the carbonate formed and/or temporal changes in the redox conditions with the basin (i.e., shifts between more oxic vs. anoxic conditions). The recorded δ13C data from LV09001 have values ranging from around 0‰ to -2.5 ‰ (PDB) with an error range of around 0.05 ‰. A cyclical trend is observed through the lithology suggesting a gradual change in relative depth and/or paleo-redox conditions at the time of deposition. Overall, the δ13C trend through LV09001 revealed systematic changes with stratigraphic depth, which seem to fluctuate in two cycles throughout the studies interval (Figure 10b).

Stratigraphic trend of $^{87}Sr/^{86}Sr$ through LV09001

Selected samples of LV09001 core were chosen for $^{87}Sr/^{86}Sr$ analysis to represent the main lithological changes and formations through the core (Figure 10). These 20 samples yielded $^{87}Sr/^{86}Sr$ ratios ranging from 0.705 to 0.735 fluctuating around a mean of 0.719 with a typical analytical error for individual samples of ±0.000003 (2 SEM). A statistically significant negative correlation ($R^2 = 0.402$) between $^{87}Sr/^{86}Sr$ and $\delta^{13}C$ values through the entire LV09001 core is observed (see Figure 15). Less radiogenic $^{87}Sr/^{86}Sr$ signals (around 0.705) correlate to $\delta^{13}C$ values close to 0‰. These are believed to reflect the most marine compositions close to the coeval open ocean, as the 'global marine' $\delta^{13}C$ and $^{87}Sr/^{86}Sr$ values based on sedimentary carbonates at the Paleo/Mesoproterozoic transition are close to 0‰ and 0.705, respectively (Schidlowski et al. 1975, Shields and Veizer 2002). Accordingly, the excursions to more negative $\delta^{13}C$ and radiogenic $^{87}Sr/^{86}Sr$ values observed in LV09001 are thus believed to reflect

more restricted paleo-depositional settings. Overall, similar to the $\delta^{13}C$ trend, the $^{87}Sr/^{86}Sr$ pattern through LV09001 also shows systematic changes with stratigraphic depth that oscillate in two cycles throughout the studies interval see Figure 10.

Stratigraphic trend of $\delta^{18}O$ through LV09001

$\delta^{18}O$ values from the LV09001 core were from the identical powder samples as the carbon isotope analysis. Overall, we observed that -9.0‰ was the most negative $\delta^{18}O$ and -3.7‰ was the most positive value from LV09001, with the mean recorded value close to -6.5‰. A large majority of the Barney Creek Formation has a $\delta^{18}O$ value at ca -6.5‰. Overall, we observe a systematic decline in $\delta^{18}O$ trend with stratigraphic depth and there is also seemingly 'secondary' signal and/or pattern superimposed on this general negative trend seen (Figure 10e).

Trace Element Concentration Through LV09001

Due to the inevitably of different sample sizes per volume of solution, and partial leaching of the bulk samples, the elemental concentrations are calculated and presented as elemental ratios normalised to calcium concentration, the latter being the major element in studied carbonates and carbonaceous shales. It was found that out of the trace elements iron, aluminium, and manganese had the highest concentration, and copper, zinc and chromium had the lowest concentrations. Barium, strontium, and phosphorus showed average concentrations. Key elements used in this study are barium and calcium (Ba/Ca ratios). Barium and calcium are commonly used for proxies in paleo-oceanographic studies indicative of paleo-productivity and organic carbon cycling in the basins (Dehairs et al. 1980, Dymond et al. 1992, Ganeshram et al. 2003, Buesseler et al. 2007). Overall, the measured Ba/Ca ratios through LV09001 range from about 1.5 to 22, and the observed Ba/Ca trend show a general negative correlation with the coeval $\delta^{13}C$ trend, and positive correlation with the radiogenic $^{87}Sr/^{86}Sr$ proxy record (see Figure 10).

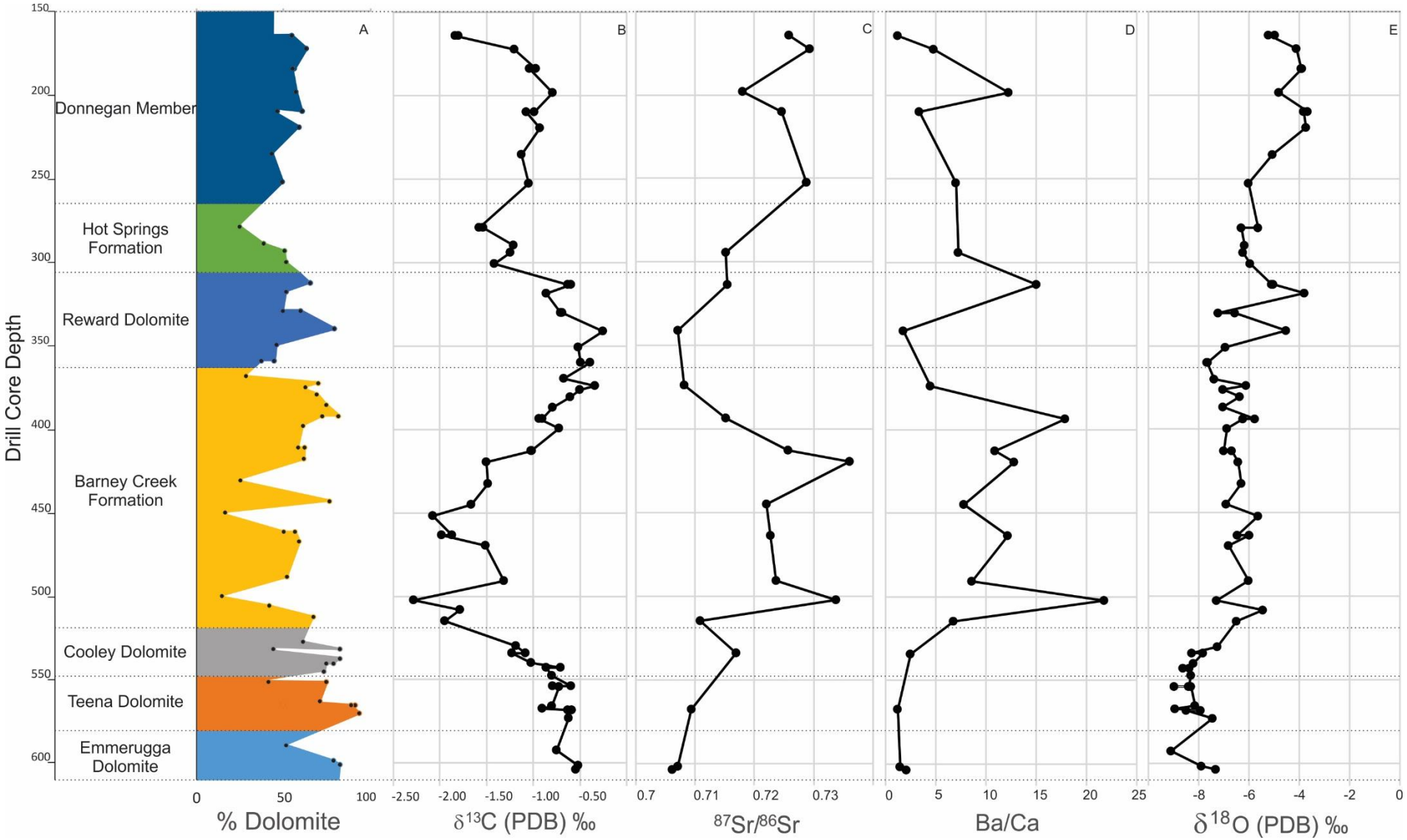

Figure 10. Depth profile of LV09001 showing percent dolomite (A), the $\delta^{13}C$ trend (B), $^{87}Sr/^{86}Sr$ trend (C), Ba/Ca elemental ratios (D), and $\delta^{18}O$ trend (E).

DISCUSSION

Interpretation of the stratigraphic $\delta^{13}C$ trend from LV09001

Carbon isotope fractionation occurs during photosynthesis, where lighter carbon isotopes (^{12}C) are preferentially taken into the organism and converted into organic material. As a result terrestrial and marine, biomass and organic matter have a typical negative $\delta^{13}C$ signature around -23‰ depending on the type of biological fixation mechanisms for carbon (O'Leary 1981, Ruby et al. 1987, Fry et al. 1991). After the formation, the carbon in the terrestrial and/or marine biomass can be converted to inorganic carbon via the respiration and decay of organic matter (i.e., oxidation of organics to CO_2). In specific marine settings where 'mineralisation' of organic carbon in sediments may occur, the process will result in $\delta^{13}C$ values of local dissolved inorganic carbon (DIC) reflecting the light carbon isotope composition of the original organic matter (i.e., DIC with $\delta^{13}C$ of about -23‰) (Figure 12). When a carbonate forms from such isotopically light DIC, they may inherit such distinctive negative $\delta^{13}C$ compositions. This composition possibly reflects the mixture between such isotopically light DIC source (-23 ‰) from the organic carbon mineralisation, and a heavier DIC typical for ambient open ocean reservoir with $\delta^{13}C$ close to 0 ‰ (Zachos et al. 1989, Kump and Arthur 1999). The amount of remineralised organic matter in a water body will affect the local $\delta^{13}C$ signal of DIC and accordingly where there is more organic matter there is also a higher chance for remineralisation and influx of light carbon into the local waters. Hence it is proposed a possible explanation for the observed excursion of heavy carbon through the carbonate record of LV09001 (i.e., negative $\delta^{13}C$ anomaly of -2.5‰) found in the Barney Creek Formation, might be related to the processes involving remineralisation of organic carbon into the sediment-water interface. Analogous to this situation is the modern Black Sea, where deeper anoxic waters

show a systematically negative $\delta^{13}C$ signature in DIC due to local organic carbon cycling and remineralisation (Fry et al., 1991).

The McArthur Basin has been proven to undergo anoxic and euxinic events (Cox et al. 2016). A simple mass balance calculation for carbon cycling can quantify the relative fraction of organic carbon into the basin, and local DIC reservoir. Accordingly, $\delta^{13}C_{Basin\ water}$ is the $\delta^{13}C$ value of the local DIC reservoir that would be present in the water column at time of carbonate formation. $\delta^{13}C_{sw}$ is the value of the global sea water DIC, which at 1600Ma is estimated to be close to 0‰ (Schidlowski et al. 1975, Kuznetsov et al. 2010) and the remineralised organic carbon flux ($\delta^{13}C_{org}$) has a $\delta^{13}C$ signature of around -23‰. Thus, the corresponding carbon isotope mass balance of local DIC and its isotope composition ($\delta^{13}C$) can be calculated according to the following equation:

$$\delta^{13}C_{Basin\ water} = (\delta^{13}C_{sw} \times F_{sw}) + (\delta^{13}C_{org} \times F_{org})$$

where F_{sw} and F_{org}, and the mass fractions of carbon (DIC) originating, respectively, from the coeval seawater and the remineralised organic carbon sources.

Using these parameters, the mass fraction of the remineralised organic carbon (F_{org}) in the basin over time can be calculated, based on the $\delta^{13}C$ record of sedimentary carbonates. The most negative $\delta^{13}C$ value in our carbonate record from LV09001 is reaching approximately -2.5‰ (Figure 10) which is also associated with an organic-rich interval in the Barney Creek Formation. Mass balance calculations show that a fraction of remineralised carbon (F_{org}) of around 10% is required to explain the observed decrease in the $\delta^{13}C$ carbonate record of about -2.5‰, assuming that the carbon isotope composition of coeval marine DIC and global seawater was constant at 0‰ (Table 1, Figure 11).

$\delta^{13}C$ Basin water ‰	$\delta^{13}C$(SW) ‰	F(SW)	$\delta^{13}C$(ORG) ‰	F(ORG)
0	**0**	**1**	**-23**	**0**
-1.15	**0**	**0.95**	**-23**	**0.05**
-2.3	**0**	**0.9**	**-23**	**0.1**
-4.6	0	0.8	-23	0.2
-6.9	0	0.7	-23	0.3
-9.2	0	0.6	-23	0.4
-11.5	0	0.5	-23	0.5
-13.8	0	0.4	-23	0.6
-16.1	0	0.3	-23	0.7
-18.4	0	0.2	-23	0.8
-20.7	0	0.1	-23	0.9
-23	0	0	-23	1

Table 1 The modelled fractions of the remineralised organic carbon (Forg) present in local DIC in the McArthur Basin. The most negative value in the Barney Creek Formation is around -2.5‰, corresponding to Forg close to 0.1 (about 10%).

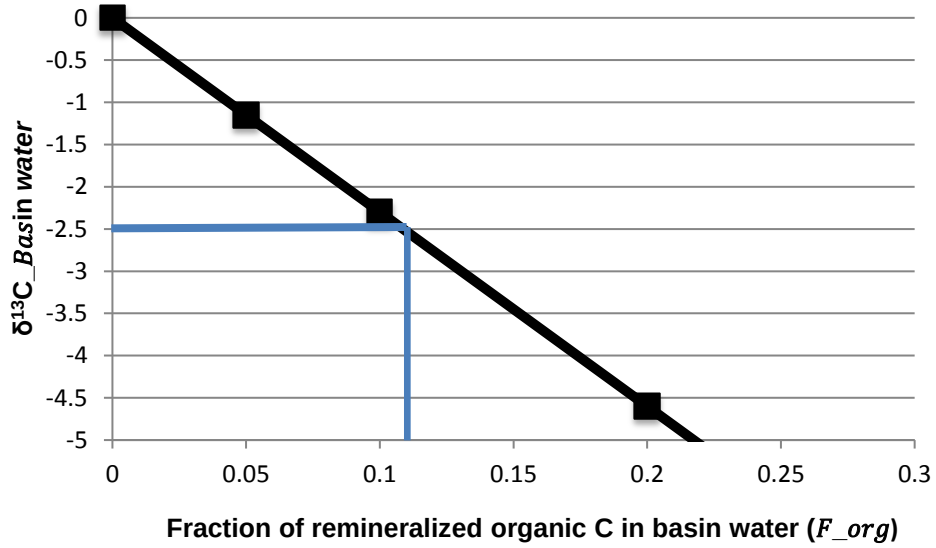

Figure 11 Calculated fractions of re-mineralised carbon (Forg) in a local DIC reservoir, needed to explain the negative anomalies observed in carbonate δ13C record. The blue line represents the most negative signal observed where the highest Forg fraction occurred, i.e., around 10%.

Constraints on depth of deposition

Another factor that could control the $\delta^{13}C$ of the dolomite is the depth of deposition. As previously stated, the McArthur Basin sediments show qualities of an anoxic inland sea similar to the modern day Black Sea (Shen et al. 2003, Brocks and Schaeffer 2008, Cox et al. 2016). As discovered with previous studies on the Black Sea, the $\delta^{13}C$ of the water column is depth dependent (Fry et al. 1991). This is explained by the remineralisation of particulate organic matter containing enriched amounts of ^{12}C. As the source of light carbon is the organic matter

present in the deep-sea sediments, the lightest $\delta^{13}C$ signal of local DIC in the Black Sea waters is at the deepest depths, i.e., close to the source of the remineralised organic carbon. Using this analogue from the Black Sea, one might predict that a carbonate with higher levels of light carbon are deposited at deeper depths, and a heavier carbon signal is representative of shallower water. However, it is also possible that changes in depositional depth are not the primary control of the observed $\delta^{13}C$ variations in LV09001. It is possible the $\delta^{13}C$ variations are due to temporal changes in the redox conditions within the basin. Temporal shifts from more oxic to anoxic conditions, rather than changes in depositional depths in a permanent redox stratified basin is a potential scenario.

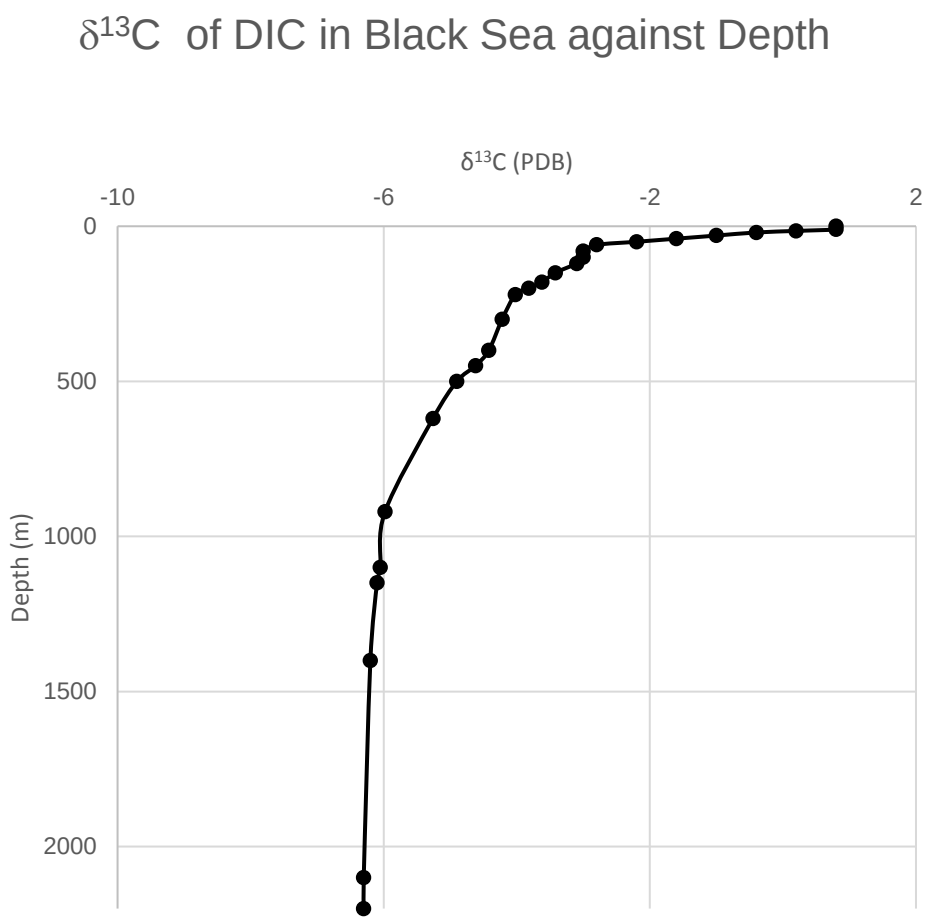

Figure 12. Changes in $\delta^{13}C$ trend in DIC from waters collected in the Black Sea, plotted as a function of water depths (modified from (Fry et al. 1991)

Interpretation of the stratigraphic $^{87}Sr/^{86}Sr$ trend from LV09001

Strontium is an alkaline earth metal with a similar ionic radius to that of calcium allowing for strontium to substitute in place of calcium in typical carbonate minerals such as dolomite, calcite and aragonite. The element rubidium has a similar radius to potassium and will substitute into potassium rich minerals for example silicates and clays. Rubidium is a lithophile element and so is a more incompatible element compared to strontium. In the situation of partial melting; Rb will partition into the melt easier than Sr, resulting in Rb depleted mantle compared to Sr, while the crust will be Rb-enriched. The radiogenic decay of rubidium ($^{87}Rb \rightarrow {}^{87}Sr + \beta^-$) will produce higher levels of radiogenic ^{87}Sr in the continental crust than the mantle and/or typical oceanic crust. Consequently, weathering of continental granitic rocks will supply to the oceans a flux of radiogenic Sr with relatively high $^{87}Sr/^{86}Sr$ signature, whereas the input of Sr from mid-ocean ridge hydrothermal system and submarine weathering/dissolution of oceanic crust will, in turn, supply to seawater less radiogenic $^{87}Sr/^{86}Sr$. Hence, changes in the balance between the continental versus submarine hydrothermal fluxes of Sr to the ocean will modulate the $^{87}Sr/^{86}Sr$ composition of seawater over geological time (Shields and Veizer 2002). Similarly, in restricted coastal settings and/or lagoonal environments, the local seawater can develop 'non-marine' $^{87}Sr/^{86}Sr$ signatures due to i) the local inputs of continentally derived radiogenic Sr, and at the same time also ii) a more restricted communication of the basin with an open ocean.

Available studies suggest that tectonic events and the associated changes in sea level and basin subsidence were responsible for changes in relative restriction of the intracratonic McArthur Basin from the coeval Proterozoic ocean (Brown et al. 1969, Jackson et al. 1987, Bull 1998a, Rawlings 1999, Shen et al. 2002, Schmid 2015). In a restricted intracratonic setting the basin is not as connected to the global ocean. Thus the local Sr isotope budget in the basin will be more dominated by the inputs of the radiogenic Sr from continental sources relative to marine

Sr sources (Sun and McDonough 1989, Jones and Jenkyns 2001). The weathering of ^{87}Sr enriched continental crust and its supply into the basin will result in an increase in a local seawater $^{87}Sr/^{86}Sr$ signature, which will be then imparted on the Sr isotope composition of carbonates that formed in the basin. A mass balance equation can be used to determine the fraction of strontium in the local basinal waters that originated from continental weathering (F_{RIV}), relative to the fraction of Sr derived from coeval open ocean or seawater (F_{SW}). Using the inferred $^{87}Sr/^{86}Sr$ signature for paleo-seawater at ca. 1600 Ma of about 0.705 (Shields and Veizer 2002, Kuznetsov et al. 2010), and a local continental weathering flux with radiogenic $^{87}Sr/^{86}Sr$ signature of 0.740 (Galy et al. 1999, Kuznetsov et al. 2010), the calculated fraction of continentally derived strontium (F_{RIV}) in the McArthur Basin and its paleo-seawater and/or local basinal waters can be calculated based on the following equation:

$$^{87}\mathrm{Sr}/^{86}\mathrm{Sr}_{BAS} = (^{87}\mathrm{Sr}/^{86}\mathrm{Sr}_{SW} \times F_{SW}) + (^{87}\mathrm{Sr}/^{86}\mathrm{Sr}_{RIV} \times F_{RIV})$$

where $^{87}Sr/^{86}Sr_{BAS}$ is the Sr isotope composition of a local basinal water, and $^{87}Sr/^{86}Sr_{SW}$ and $^{87}Sr/^{86}Sr_{RIV}$ are, respectively, the corresponding Sr isotope compositions of the coeval open ocean (i.e., global seawater signature) and the riverine weathering input into the basin. Below are calculated variations in $^{87}Sr/^{86}Sr_{BAS}$ as a function of different F_{RIV} fractions, which could explain most of the variability in $^{87}Sr/^{86}Sr$ data that we observe in LV09001 core (Figure 13, Table 2)

$^{87}Sr/^{86}Sr_{Bas}$	$^{87}Sr/^{86}Sr_{sw}$	F_{sw}	$^{87}Sr/^{86}Sr_{RIV}$	F_{RIV}
0.705	0.705	1	0.74	0
0.70675	0.705	0.95	0.74	0.05
0.7085	0.705	0.9	0.74	0.1
0.712	0.705	0.8	0.74	0.2
0.7155	0.705	0.7	0.74	0.3
0.719	0.705	0.6	0.74	0.4
0.7225	0.705	0.5	0.74	0.5
0.726	0.705	0.4	0.74	0.6
0.7295	0.705	0.3	0.74	0.7
0.733	0.705	0.2	0.74	0.8
0.7365	0.705	0.1	0.74	0.9
0.74	0.705	0	0.74	1

Table 2 The calculated Sr isotope composition of local basinal waters ($^{87}Sr/^{86}Sr_{BAS}$) and the corresponding fractions of riverine and/or continental derived Sr (F_{RIV}). The minimum ratio recorded was in the Emmerugga Dolomite at 0.7062, and the maximum value was in the Barney Creek Formation at 0.736.

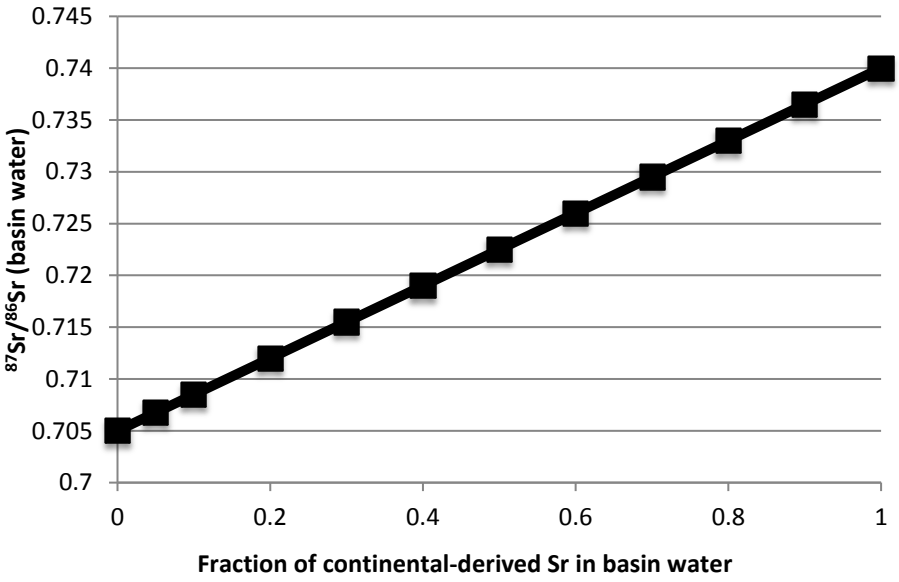

Figure 13. The Sr isotope composition of local basinal waters ($^{87}Sr/^{86}Sr_{BAS}$) plotted against the corresponding fractions of riverine and/or continental derived Sr (F_{RIV}). Riverine and/or continental input has an $^{87}Sr/^{86}Sr$ signature of 0.740, and the open ocean has an $^{87}Sr/^{86}Sr$ signature of 0.705 (Shields and Veizer 2002, and Kuznetsov et al. 2010).

Accordingly, more radiogenic $^{87}Sr/^{86}Sr$ values (> 0.710) values such as those recorded in the Barney Creek Formation and Donnegan Member Carbonates (Figure 10) indicate that the local depositional environment was significantly restricted with minimal communication with the coeval ocean water. In contrast, less radiogenic values (i.e., between 0.705 and 0.708), such as

those in Emmerggua, Teena and Reward Dolomites (see Figure 10), indicate more marine conditions and times when the basin communicated with the open ocean.

However, it should be mentioned that the more radiogenic $^{87}Sr/^{86}Sr$ values are also generally associated with intervals that are relatively carbonate-poor and organic/shale rich (i.e., with lower wt% of dolomite, such as the Barney Creek Formation.), compared to more 'marine' values present in relatively pure Emmerggua, Teena and Reward Dolomites. (Figure 4, Figure 5, Figure 6, Figure 7, Figure 10a) Thus, part of the radiogenic enrichment in these dolomite-poor samples might be due to a contribution of a radiogenic Sr leached from the silicate/clay faction present in the bulk sample. These 'secondary contamination' effects have been minimised in this study by leaching the samples at room temperatures and in weak acids (see Methods, and (Shields and Veizer 2002, Kuznetsov et al. 2010).

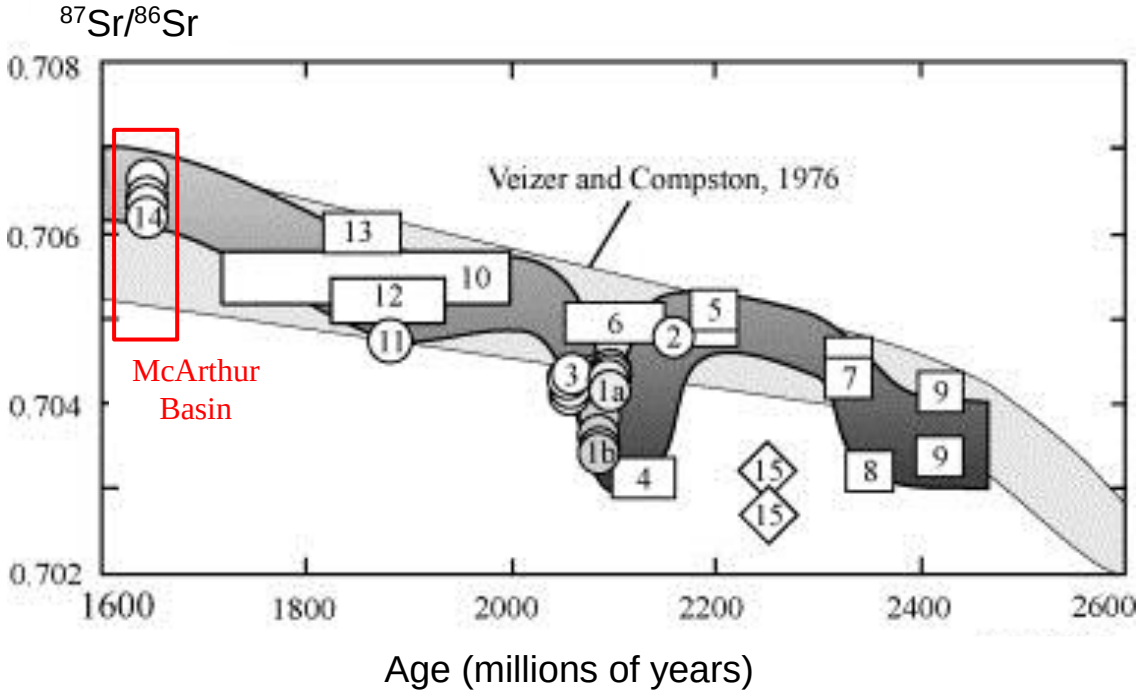

Figure 14 Inferred temporal evolution of $^{87}Sr/^{86}Sr$ Palaeoproterozoic seawater based on the analysis of well-preserved marine sedimentary carbonates (Kuznetsov et al. 2010)

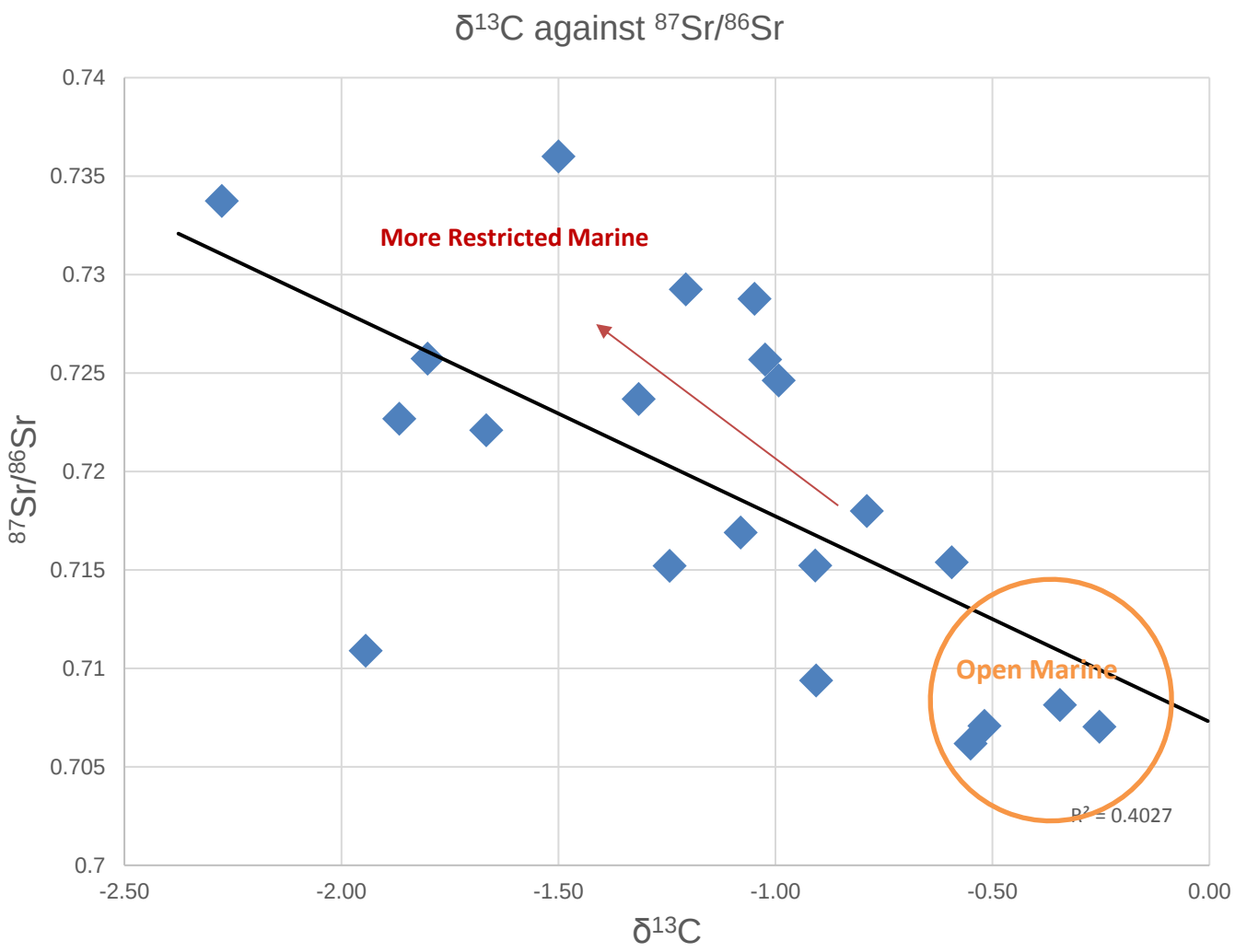

Figure 15 A cross plot of the measured isotope signals $\delta^{13}C$ and $^{87}Sr/^{86}Sr$. The least radiogenic $^{87}Sr/^{86}Sr$ signals of about 0.706 are in good agreement with the inferred paleo-seawater Sr isotope composition at 1600 Ma (see Kuznetsov et al., 2010, and Figure 14). Importantly, the corresponding $\delta^{13}C$ signatures (at $^{87}Sr/^{86}Sr$ of 0.706) is very close to 0‰ (PDB), which is interpreted here as the most marine C isotope composition recorded in McArthur Basin. Importantly, paleo-seawater $\delta^{13}C$ signatures close to 0‰ are also in good agreement with other published data for global marine $\delta^{13}C$ trend at 1600 Ma (see the Precambrian marine carbonate isotope database: Version 1.1 (Shields and Veizer 2002).

Interpretation of the stratigraphic $\delta^{18}O$ trend from LV09001

Oxygen isotopes in carbonates are very sensitive to alteration by diagenetic fluid due to the high content of oxygen in the waters. The $\delta^{18}O$ data for LV09001 has an overall decreasing trend with depth that could be explained by the effect of increasing burial temperatures with depth, following a local geothermal gradient. It has been proposed that the water-dolomite fractionation factor of oxygen ($\Delta^{18}O$) can provide a sensitive paleo-thermometer for dolomite formation (Temperature = -5.1046* $\Delta^{18}O$ +184.35) (Vasconcelos et al. 2005). Calculations on dolomite formed under laboratory conditions demonstrate that at higher temperatures the dolomite precipitate will be depleted in ^{18}O due to the fractionation of oxygen from the water into the dolomite. Based on the studies of Vasconcelos et al. (2005), the observed difference between a porewater or dolomitising fluid and precipitated dolomite is around 28.74 ‰(PDB) (at typical earth's surface temperatures close to 20 ºC). We use this difference to calculate an inferred $\delta^{18}O$ for the dolomitising fluid for LV09001 by subtracting 28.7‰ from the youngest sample, resulting in an inferred fluid $\delta^{18}O$ of -33.96‰. We then use this value to calculate the difference of $\delta^{18}O$ between the dolomite and the fluid ($\Delta^{18}O$) through depth. We then convert to burial temperatures (based on the equation shown above from Vasconcelos et al., 2005). Inferred burial temperature (or recrystalisation temperature) for dolomites can then be can then be plotted as a function of depths, and compared with the temperatures based on a local geothermal gradient. As shown in Figure 16, the inferred burial temperature agrees relatively well with the local average geothermal gradient of about 3.3 ºC increase per 100 metres of depth (Schmid 2015). Over-printed on this general negative $\delta^{18}O$ 'possible burial temperature trend' is a pattern of secondary $\delta^{18}O$ oscillations, which might reflect past changes in paleo-environmental conditions during dolomite formation. Hence, we explore this option by comparing the 'detrended' $\delta^{18}O$ data from LV09001 (i.e., where the burial temperature $\delta^{18}O$ signal have been removed, see the orange line in Figure 16), with other paleo-environmental

proxies such as C isotopes. Interestingly, when plotted against depth the detrended $\delta^{18}O$ data and $\delta^{13}C$ data appear to correlate with each other (see Figure 17), suggesting that the 'secondary' pattern in oxygen isotope data – superimposed on the generally decreasing $\delta^{18}O$ trend – might be indeed related to past paleo-environmental conditions during dolomite formation. An explanation could be local temperature changes and/or changes in $\delta^{18}O$ of local seawater, related to degree of evaporation vs. fresh water input into the basin. Although highly speculative at this stage, the heavy $\delta^{18}O$ anomalies in the detrended oxygen isotope record are generally coupled with negative $\delta^{13}C$ anomalies and also the more radiogenic $^{87}Sr/^{86}Sr$ values. Indicative of a more restricted depositional setting, it is plausible that in these restricted settings the heavy $\delta^{18}O$ anomalies could reflect more evaporation of local basinal waters in such restricted and/or lagoonal settings.

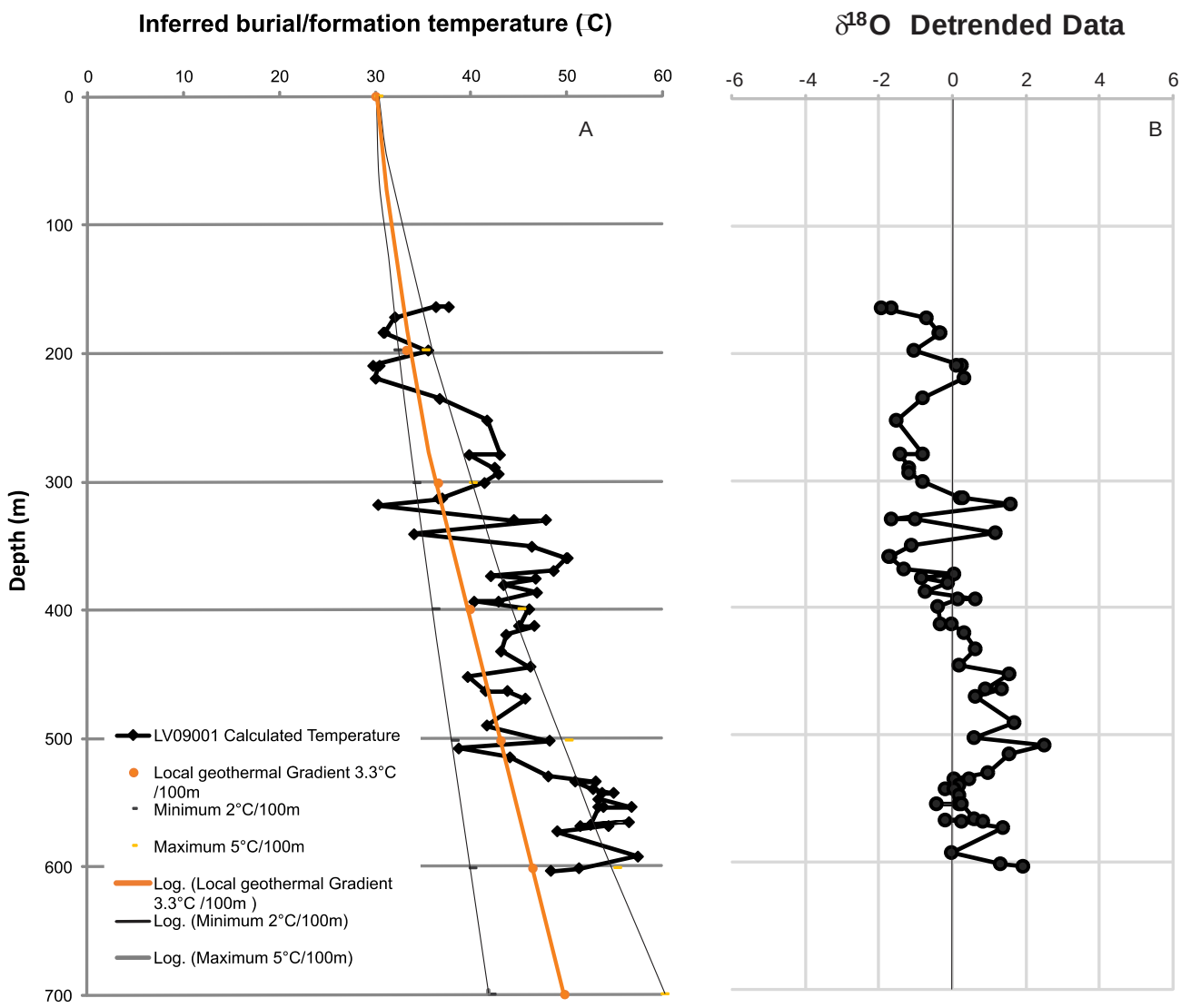

Figure 16 (Right) The inferred burial temperatures, calculated based on oxygen isotope data from LV09001 using the paleo-temperature equation of Vasconcelos et al. (2005), and minimum, maximum, and average local geothermal gradients. (Left) The detrended oxygen data from LV09001 generated by removing the linear $\delta^{18}O$ trend, which is believed to reflect primarily the burial temperature signal related to local geothermal gradient of ca. 3.3 ºC per 100 metres.

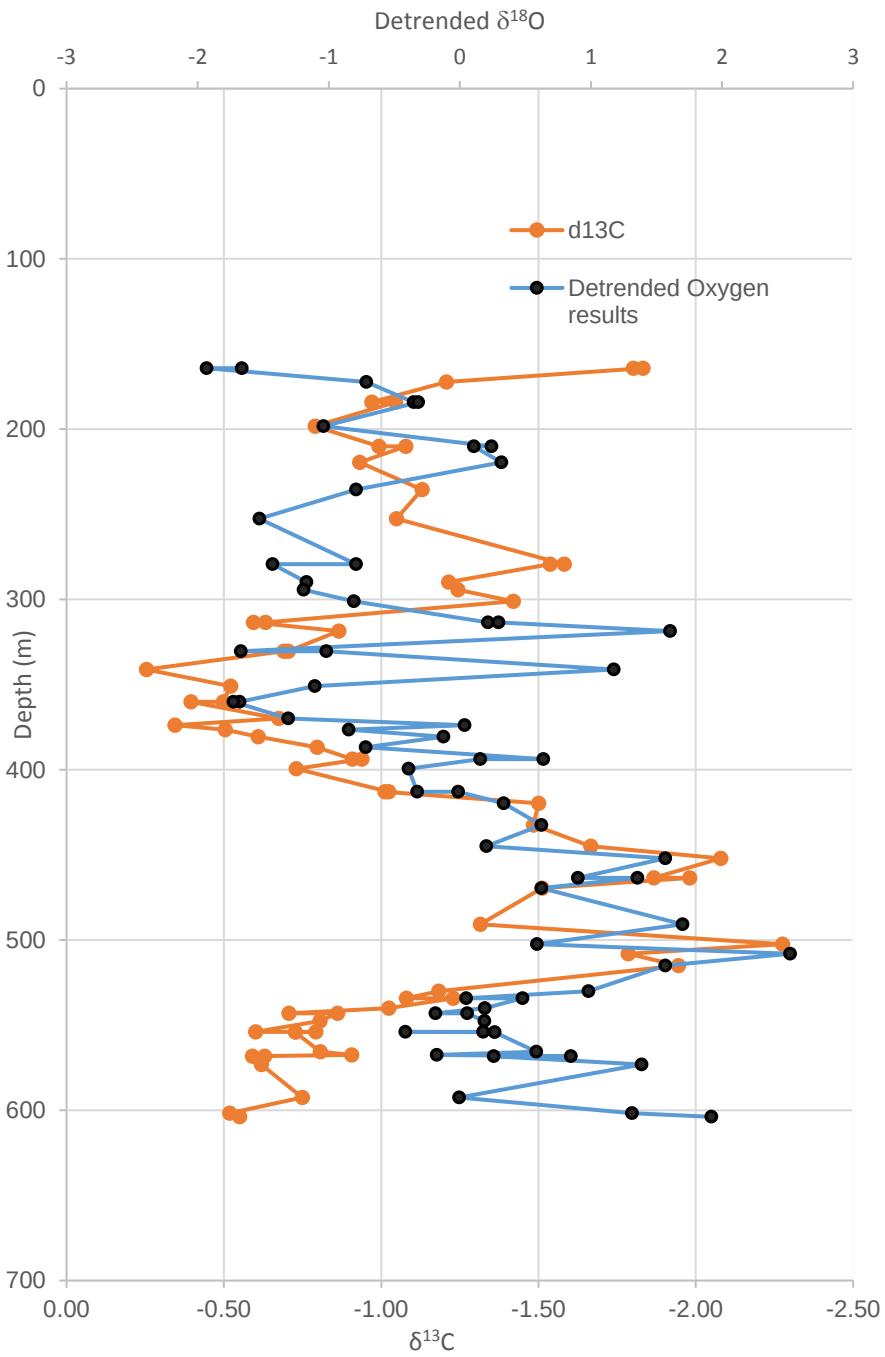

Figure 17 A plot of detrended $\delta^{18}O$ data, as well as $\delta^{13}C$ data from LV090001 as a function of depths showing a pattern of correlation, but also decoupling in certain intervals.

Interpretation of the stratigraphic Ba/Ca trend in LV09001

The behaviour of barium concentration in sea water has been intensively studied due to the element's potential to indicate bio-productivity in the oceans (Dehairs et al. 1980, Dymond et al. 1992, Ganeshram et al. 2003, Buesseler et al. 2007). The formation of barite ($BaSO_4$) in surface ocean water is biologically controlled, as normal seawater is typically 'undersaturated' with respect to barite (Paytan and Griffith 2007). Hence, the formation of barite in seawater and the associated flux of Ba to the ocean floor are linked to primary biological productivity in surface water and the formation/dissolution of barite within the water column and sediments. In the Ba/Ca trend from LV09001, we observe systematic changes that follow movements in the $\delta^{13}C$ and $^{87}Sr/^{86}Sr$ trends, suggesting that the observed Ba/Ca variations are also linked to changes in paleo-depositional environment and the bio-productivity within the basin.

Microscopy

A multitude of geochemical information was gathered from microscope observations in petrography and XRF elemental mapping. A main observation from the elemental maps created was the multiple styles of carbonate formation. The deeper units such as the Teena Dolomite had large carbonate clasts in a silicified matrix showing a low energy marine shelf for carbonate formation (Figure 4). Overlying units demonstrate different environments less favourable for carbonates to form, and so are more siliceous showing the conforming of carbonate around silicate grains (Figure 5, Figure 6). Observations on the Barney Creek Formation indicate a low energy deposition and the high degree of pyrite found throughout the unit indicates anoxic water conditions at the bottom of the basin at the time of deposition (Figure 8) (Boesen and Postma 1988, Shen et al. 2003).

Interpretation of Depositional Environment of Barney Creek Formation in LV09001

Through our work, we have created a multiproxy isotope approach based on $^{87}Sr/^{86}Sr$ and $\delta^{13}C$ tracers helping to constrain the depositional setting for one of the world's oldest hydrocarbon source rocks. Observed trends in the LV09001 core strongly indicate for the restriction of the McArthur Basin during the deposition of the Barney Creek Formation. Relative $\delta^{13}C$ signals and Ba/Ca concentrations of the Barney Creek Formation point toward an increase of organic matter collecting in the basin, a plausible scenario in a restricted marine setting. Radiogenic strontium isotope data also indicates a restriction in the basin, with an $^{87}Sr/^{86}Sr$ signal indicating a larger fraction of continental runoff comparative to an open marine style setting.

Correlation

Using isotopic signatures of carbon, we have observed a preliminary correlation factor for stratigraphy in the McArthur Basin. Using $\delta^{13}C$ signatures from LV09001 as a reference, similar signatures found in other wells can be indicative of matching depositional environments. The 2.5‰ (PDB) magnitude excursion found in the Barney Creek Formation is seen in other sampled drill core across the McArthur Group up to 100 km away (McA 5, Bj2. See Figure 18). Future research will be conducted on core samples from BCF4 & 4a to test the extent of a possible isotopic intrabasin correlation technique.

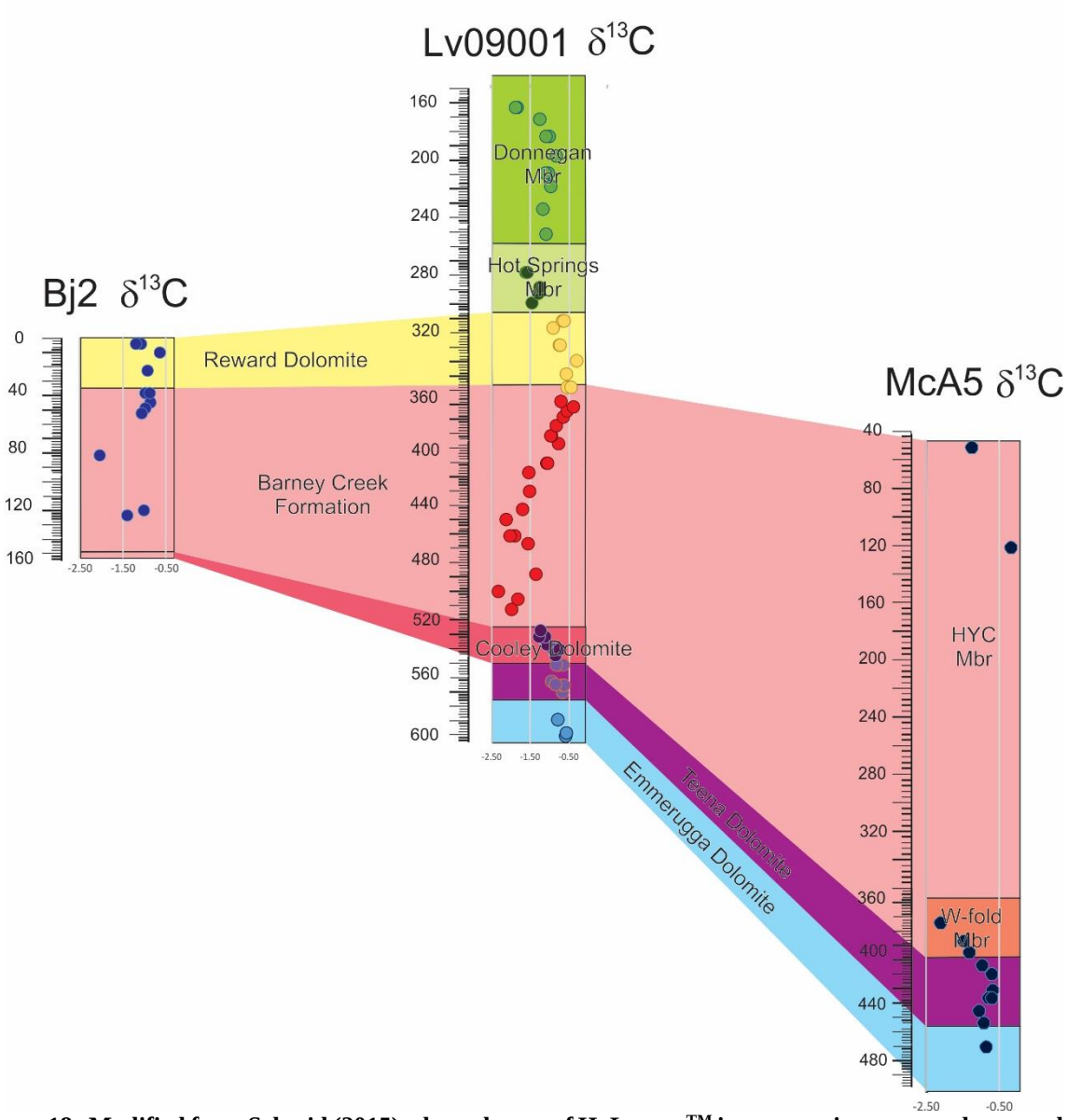

Figure 18. Modified from Schmid (2015) where the use of HyLogger™ interpretations are used to correlate different cores within the basin. Our preliminary $\delta^{13}C$ data is overlain on the formations.

CONCLUSIONS

Stable and radiogenic isotope data ($\delta^{13}C$, $\delta^{18}O$, $^{87}Sr/^{86}Sr$) and elemental concentrations (Ba/Ca) presented in this paper from the high-resolution sampling of the LV09001 core has helped to constrain the changing depositional environment throughout the Glyde Package in the McArthur Group.

- Fluctuating carbon isotope ratios through stratigraphy in the Glyde Package are indicative of changes in the local carbon cycling through time, specifically suggested

changes in the fraction of the remineralised of organic carbon input into the basin due to the decay and remineralisation of organic matter, the latter believed to be the primary cause for the -2.5‰ (PDB) anomaly in the Barney Creek Formation.

- Ba/Ca data correlating to the measured $\delta^{13}C$ curve, is also an indicative of changes in local cycling and decay of organic matter in the basin. The higher concentration of barium in the Barney Creek Formation point toward an increase of organic matter collecting in the basin.
- Radiogenic strontium-isotope signal ($^{87}Sr/^{86}Sr$) are proxy for weathering and input of radiogenic Sr from continents, and thus local restriction of the basin. It was found that the units with lower radiogenic signals close to 0.705 (open marine environments) correlate with $\delta^{13}C$ close to 0‰ PDB and low concentrations of barium. High radiogenic signals 0.73 (restricted marine) correlate with negative anomalies in $\delta^{13}C$ and increased barium concentrations.
- The use of this multi-proxy approach has helped to constrain the paleo-depositional environment of the Glyde Package dated at ca. 1600 to 1640 Ma. Our data describes a setting of a regressive basin becoming more restricted to open-marine water. The restriction causes basin stratification creating anoxic bottom water conditions and a lack of mixing allows for the accumulation of organic matter in the basin observed in the sediments.

ACKNOWLEDGMENTS

I would firstly like to thank my supervisor Dr Juraj Farkas for his amazing knowledge of geochemistry and isotopes. I appreciate all the support and guidance you gave me throughout the year. Alan Collins, Todd Smith and Bo Yang for being part of the McArthur Team and providing great enjoyment and support in the field. Thank you to the Santos Team for their

input and investment in this project. The people at NTGS for their remarkable dedication to the pursuit and sharing of geological knowledge of the Northern Territory. The staff of Adelaide University, who helped me along the way with general queries, motivational anecdotes about their honours experiences, intensive laboratory support, and friendly chit-chat. You guys do an amazing job. Adelaide Microscopy for allowing us to use their incredible equipment. Special thanks to my family for pushing me through the year and always being concerned about my fluctuating mood, health, weight, diet and sleeping patterns. Katie Howard has been a great source of instant advice, consultation and entertainment this year, and has kept the honours cohort in line and on track no matter how feral we became. And finally the honours cohort, what a bunch of legends, thanks for all the help this year, from computer program advice to fashion advice, you guys have always been there with a smile (most of the time).

REFERENCES

AHMAD M. & DUNSTER J. 2013 Chapter 15: McArthur Basin: in Ahmad M and Munson TJ (compilers).', *Geology and mineral resources of the Northern Territory'. Northern Territory Geological Survey, Special Publication,* **5**.

BETTS P., ARMIT R., STEWART J., AITKEN A., AILLERES L., DONCHAK P., HUTTON L., WITHNALL I. & GILES D. 2016 Australia and Nuna, *Geological Society, London, Special Publications,* **424**, 47-81.

BOESEN C. & POSTMA D. 1988 Pyrite formation in anoxic environments of the Baltic, *American Journal of Science,* **288**, 575-603.

BROCKS J. J. & SCHAEFFER P. 2008 Okenane, a biomarker for purple sulfur bacteria (Chromatiaceae), and other new carotenoid derivatives from the 1640 Ma Barney Creek Formation, *Geochimica et Cosmochimica Acta,* **72**, 1396-1414.

BROWN M., CLAXTON C. & PLUMB K. 1969 The Proterozoic Barney Creek Formation and some associated units of the McArthur Group, *Northern Territory, Australia: Bureau of Mineral Resources Record,* **145**, p.59.

BUESSELER K. O., LAMBORG C. H., BOYD P. W., LAM P. J., TRULL T. W., BIDIGARE R. R., BISHOP J. K., CASCIOTTI K. L., DEHAIRS F. & ELSKENS M. 2007 Revisiting carbon flux through the ocean's twilight zone, *science,* **316**, 567-570.

BULL S. 1998a Sedimentology of the Palaeoproterozoic Barney Creek formation in DDH BMR McArthur 2, southern McArthur Basin, northern territory, *Australian Journal of Earth Sciences,* **45**, 21-31.

BULL S. W. 1998b Sedimentology of the Palaeoproterozoic Barney Creek formation in DDH BMR McArthur 2, southern McArthur basin, northern territory, *Australian Journal of Earth Sciences,* **45**, 21-31.

COX G. M., JARRETT A., EDWARDS D., CROCKFORD P. W., HALVERSON G. P., COLLINS A. S., POIRIER A. & LI Z.-X. 2016 Basin redox and primary productivity within the Mesoproterozoic Roper Seaway, *Chemical Geology,* **440**, 101-114.

DAVIDSON G. J. & DASHLOOTY S. A. 1993 The Glyde Sub-basin: A volcaniclastic-bearing pull-apart basin coeval with the McArthur River base-metal deposit, Northern Territory, *Australian Journal of Earth Sciences,* **40**, 527-543.

DEHAIRS F., CHESSELET R. & JEDWAB J. 1980 Discrete suspended particles of barite and the barium cycle in the open ocean, *Earth and Planetary Science Letters,* **49**, 528-550.

DYMOND J., SUESS E. & LYLE M. 1992 Barium in deep-sea sediment: A geochemical proxy for paleoproductivity, *Paleoceanography,* **7**, 163-181.

FARKAS. J. C. R., JACOBSEN. S.B., KUMP. L.R., MELEZHIK, V.A. 2013 Ca and Mg isotopes in sedimentary carbonates. *In* SPRINGER ed. *The Archive of Earths Oxygenation.* pp. 1468-1482, Springer,

FRY B., JANNASCH H. W., MOLYNEAUX S. J., WIRSEN C. O., MURAMOTO J. A. & KING S. 1991 Stable isotope studies of the carbon, nitrogen and sulfur cycles in the Black Sea and the Cariaco Trench, *Deep Sea Research Part A. Oceanographic Research Papers,* **38**, S1003-S1019.

GALY A., FRANCE-LANORD C. & DERRY L. A. 1999 The strontium isotopic budget of Himalayan rivers in Nepal and Bangladesh, *Geochimica et Cosmochimica Acta,* **63**, 1905-1925.

GANESHRAM R. S., FRANÇOIS R., COMMEAU J. & BROWN-LEGER S. L. 2003 An experimental investigation of barite formation in seawater, *Geochimica et Cosmochimica Acta,* **67**, 2599-2605.

JACKSON M., MUIR M. & PLUMB K. 1987 Geology of the southern McArthur Basin, Northern Territory. Australian Government Publishing Service.

JACKSON M. & SOUTHGATE P. 2000 Evolution of three unconformity-bounded sandy carbonate successions in the McArthur River region of northern Australia: The Lawn, Wide and Doom Supersequences in a proximal part of the Isa Superbasin, *Australian Journal of Earth Sciences,* **47**, 625-635.

JONES C. E. & JENKYNS H. C. 2001 Seawater strontium isotopes, oceanic anoxic events, and seafloor hydrothermal activity in the Jurassic and Cretaceous, *American Journal of Science,* **301**, 112-149.

KELLY A., LOVE G., LYONS T. & ANBAR A. 2010 An integrated organic-inorganic geochemical study of the 1.64 Ga Barney Creek Formation in Australia. AGU Fall Meeting Abstracts. pp. 0429.

KUMP L. R. & ARTHUR M. A. 1999 Interpreting carbon-isotope excursions: carbonates and organic matter, *Chemical Geology,* **161**, 181-198.

KUZNETSOV A., MELEZHIK V., GOROKHOV I., MELNIKOV N., KONSTANTINOVA G., KUTYAVIN E. & TURCHENKO T. 2010 Sr isotopic composition of Paleoproterozoic 13 C-rich carbonate rocks: the Tulomozero Formation, SE Fennoscandian Shield, *Precambrian Research,* **182**, 300-312.

LINDSAY J. & BRASIER M. 2000 A carbon isotope reference curve for ca. 1700–1575 Ma, McArthur and Mount Isa Basins, Northern Australia, *Precambrian Research,* **99**, 271-308.

LOGAN R. & WILLIAMS N. 1984 Sedimentary controls on the hydrothermal system that formed the HYC deposit at McArthur River, Northern Territory. Geological Society of Australia Abstracts. pp. 339-340.

MELEZHIK V. A., FALLICK A. E., RYCHANCHIK D. V. & KUZNETSOV A. B. 2005 Palaeoproterozoic evaporites in Fennoscandia: implications for seawater sulphate, the rise of atmospheric oxygen and local amplification of the δ13C excursion, *Terra Nova,* **17**, 141-148.

O'LEARY M. H. 1981 Carbon isotope fractionation in plants, *Phytochemistry,* **20**, 553-567.

OEHLER J. H. 1977 Microflora of the HYC pyritic shale member of the Barney Creek Formation (McArthur Group), middle Proterozoic of northern Australia, *Alcheringa,* **1**, 315-349.

PAGE R., JACKSON M. & KRASSAY A. 2000 Constraining sequence stratigraphy in north Australian basins: SHRIMP U–Pb zircon geochronology between Mt Isa and McArthur River, *Australian Journal of Earth Sciences,* **47**, 431-459.

PAGE R. W. & SWEET I. P. 1998 Geochronology of basin phases in the western Mt Isa Inlier, and correlation with the McArthur Basin, *Australian Journal of Earth Sciences,* **45**, 219-232.

PAYTAN A. & GRIFFITH E. M. 2007 Marine barite: Recorder of variations in ocean export productivity, *Deep Sea Research Part II: Topical Studies in Oceanography,* **54**, 687-705.

RAWLINGS D. 1999 Stratigraphic resolution of a multiphase intracratonic basin system: the McArthur Basin, northern Australia, *Australian Journal of Earth Sciences,* **46**, 703-723.

RUBY E. G., JANNASCH H. W. & DEUSER W. G. 1987 Fractionation of stable carbon isotopes during chemoautotrophic growth of sulfur-oxidizing bacteria, *Applied and Environmental Microbiology,* **53**, 1940-1943.

SCHIDLOWSKI M., EICHMANN R. & JUNGE C. E. 1975 Precambrian sedimentary carbonates: carbon and oxygen isotope geochemistry and implications for the terrestrial oxygen budget, *Precambrian Research,* **2**, 1-69.

SCHMID S. 2015 Sedimentological review of the Barney Creek Formation in drillholes LV09001, BJ2, McA5, McArthur Basin.

SHEN Y., CANFIELD D. E. & KNOLL A. H. 2002 Middle Proterozoic ocean chemistry: evidence from the McArthur Basin, northern Australia, *American Journal of Science,* **302**, 81-109.

SHEN Y., KNOLL A. H. & WALTER M. R. 2003 Evidence for low sulphate and anoxia in a mid-Proterozoic marine basin, *Nature,* **423**, 632-635.

SHIELDS G. & VEIZER J. 2002 Precambrian marine carbonate isotope database: Version 1.1, *Geochemistry, Geophysics, Geosystems,* **3**.

SUN S.-S. & MCDONOUGH W.-S. 1989 Chemical and isotopic systematics of oceanic basalts: implications for mantle composition and processes, *Geological Society, London, Special Publications,* **42**, 313-345.

VAN BREUGEL Y., SCHOUTEN S., PAETZEL M., NORDEIDE R. & DAMSTÉ J. S. 2005 The impact of recycling of organic carbon on the stable carbon isotopic composition of dissolved inorganic carbon in a stratified marine system (Kyllaren fjord, Norway), *Organic geochemistry,* **36**, 1163-1173.

VASCONCELOS C., MCKENZIE J. A., WARTHMANN R. & BERNASCONI S. M. 2005 Calibration of the δ18O paleothermometer for dolomite precipitated in microbial cultures and natural environments, *Geology,* **33**, 317-320.

ZACHOS J. C., ARTHUR M. A. & DEAN W. E. 1989 Geochemical evidence for suppression of pelagic marine productivity at the Cretaceous/Tertiary boundary.

APPENDIX A:

EXTENDED METHODS

Carbon, Oxygen, Carbonate

Solution ICPMS

TIMS $^{87}Sr/^{86}Sr$

Solutions with purified Sr fraction were dropped on parafilm before pipetting and loading. Centre filaments with non-zone-refined Re ribbon was used, no inner or outer filaments were used.

1. Load 1 µL 1M H_3PO_4 and evaporate at 0.5-0.8 A.
2. Load 0.5 µL Bircks Solution and evaporate at 0.5 A.
3. Load ~500ng Sr in 1 µL Bircks Solution and dry st 0.5 A.
4. Gradually increase to ~1 A, but reduce current if load starts to spread.
5. Over about 1 minute, increase to 1.8 A and leave for 1 minute.
6. Heat to just red for several seconds, estimated at ~2.3-2.4 A.

Turn down the current and fix the filament onto the magazine, record sample names and details, corresponding to the position of the filaments.

In the mass spectrometer, the ionisatoin (centre) filament current was ramped slowly to 2.3 A, about 30 minutes, then the current was turned up slowly to ~3.1-3.3 A, resulting in an ionisation temperature of ~1350-1400^{o}C and a target ion beam intensity of ~5-6 A (88Sr).

Photomicrographs and thin sections

Sample	Formation	Thin Section	Lithology description	Depth
Lv1	Emmerugga Dolostone	 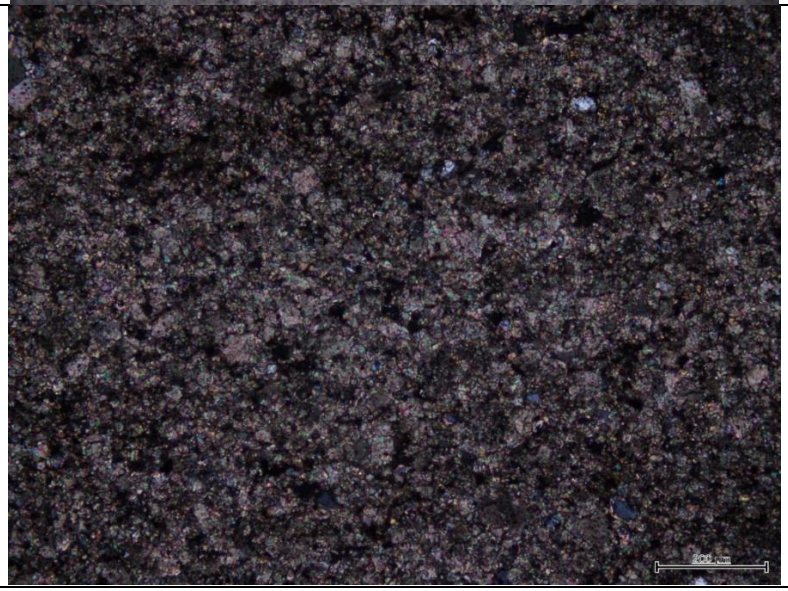	Grainy Micrite. Massive dark grey dolostone. Medium to fine grained mudstone matrix.	603.83

Sample	Formation	Thin Section	Lithology description	Depth
Lv3	Emmerugga Dolostone	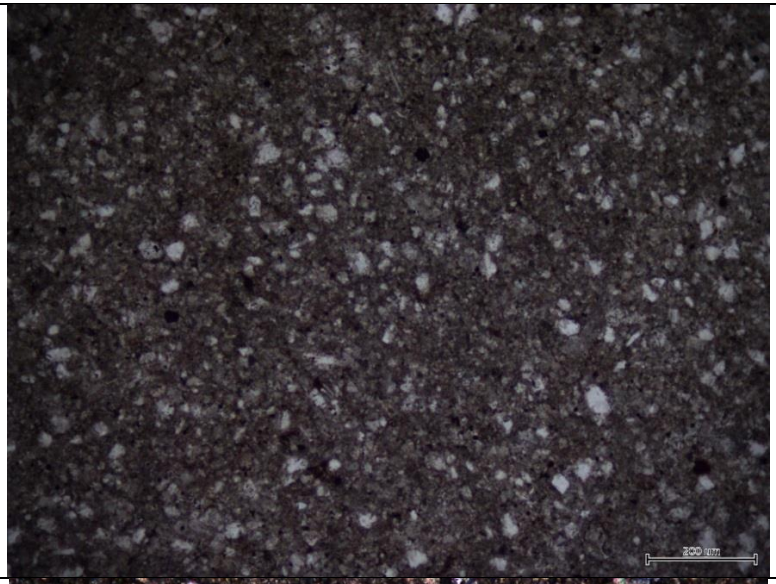 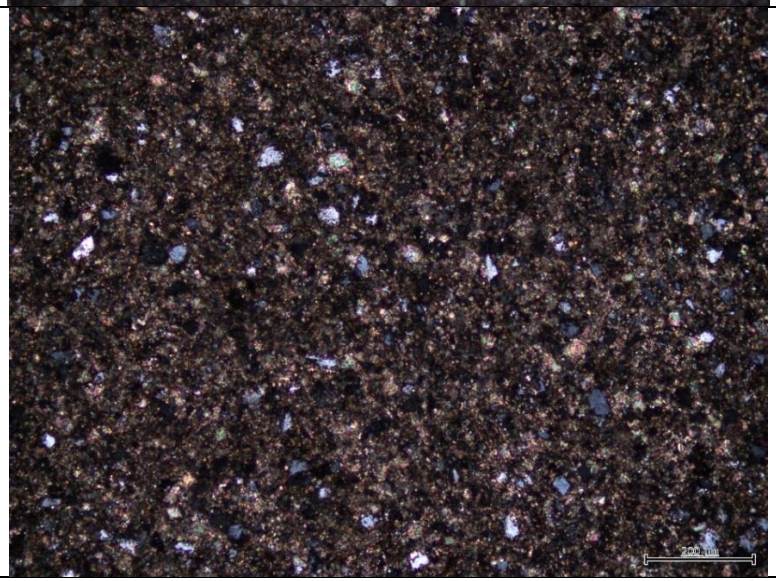		592.48

Sample	Formation	Thin Section	Lithology description	Depth
Lv5	Teena Dolomite	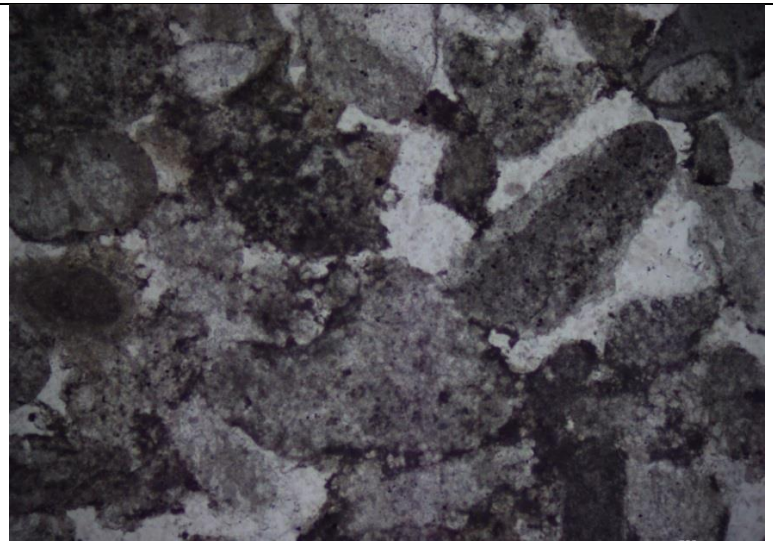 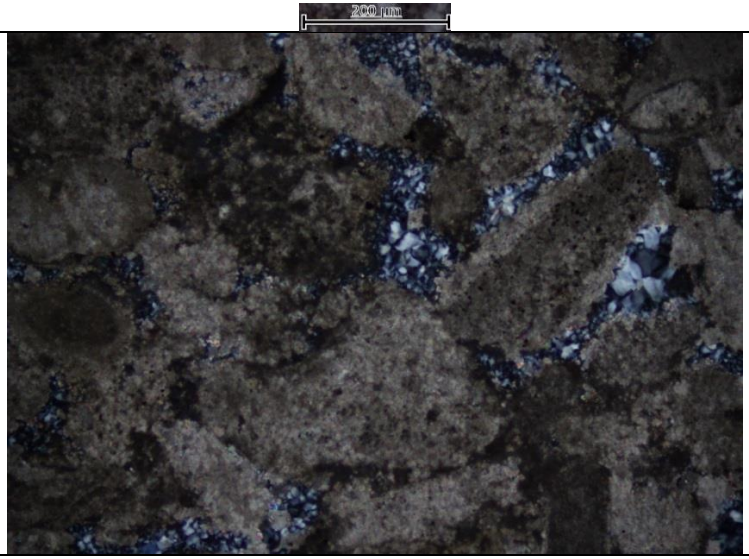	Large, rounded, dolomite clasts. Grain supported in a silicified clay matrix.	568.28

Sample	Formation	Thin Section	Lithology description	Depth
LV11	Cooley Dolostone	 	Dolomitic siltstone. finely laminated, grain packed micrite	543

Sample	Formation	Thin Section	Lithology description	Depth
LV13	Cooley Dolostone	 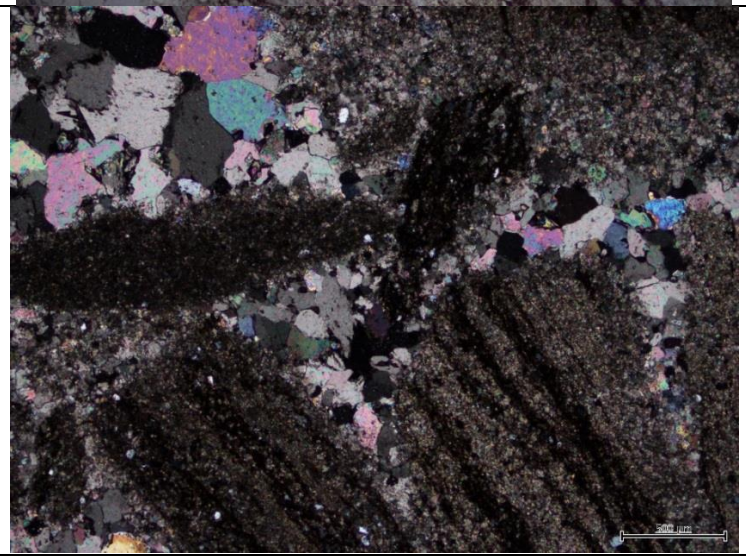	Chaotic, coarse, breccia in a calcite matrix. Clasts are a mix of lower units from homogenous Emmerugga, Teena and finely layered Cooley dolostones.	534.25

Sample	Formation	Thin Section	Lithology description	Depth
Lv32	Barney Creek Formation	 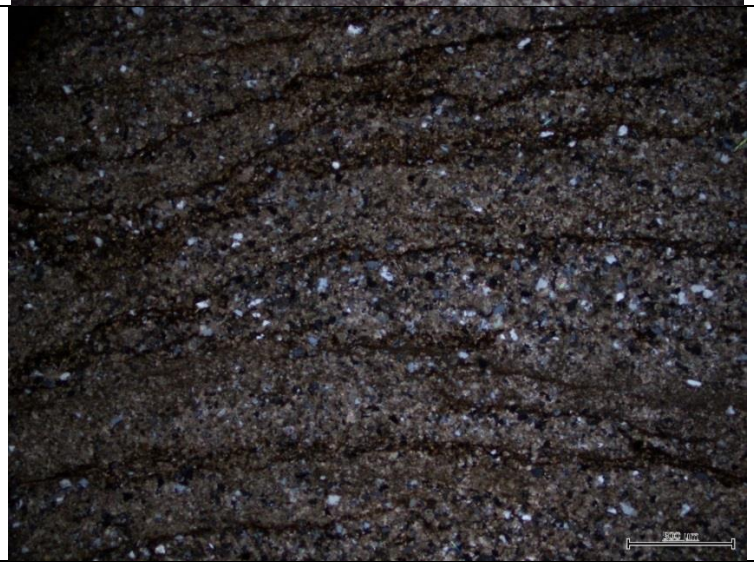	Interbedded organic siltstone with fine dolomitic clasts in a slightly silicified clay matrix.	380.7

Sample	Formation	Thin Section	Lithology description	Depth
Lv37	Reward Dolostone	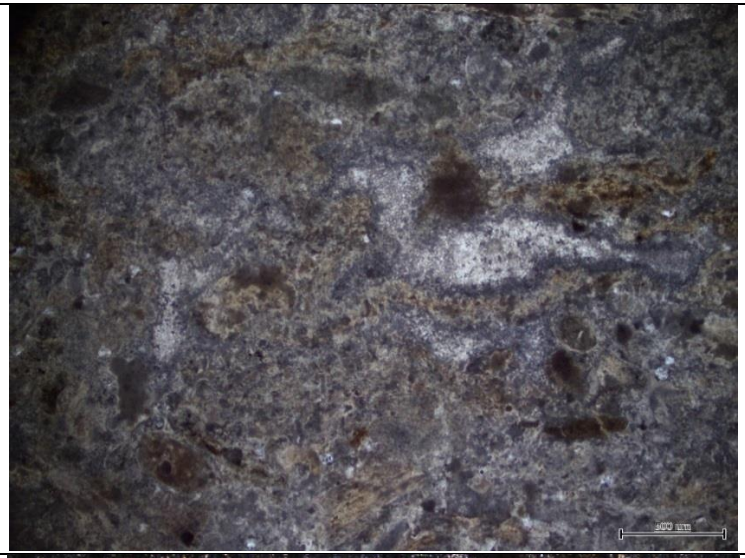 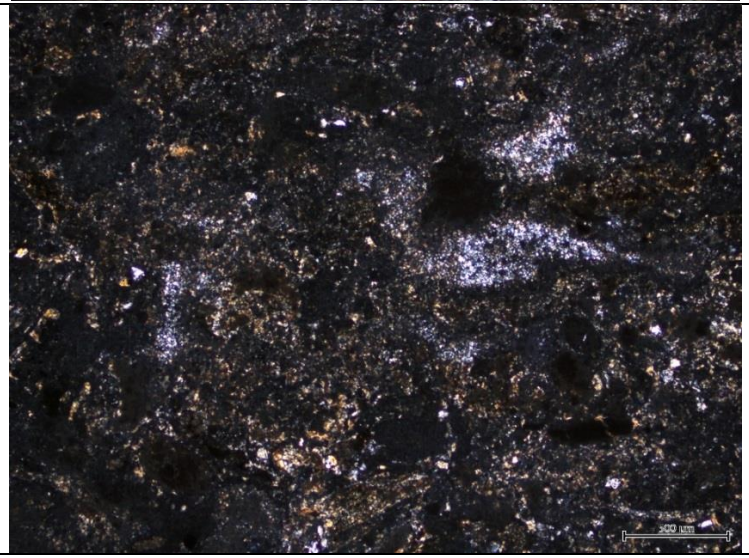		350.9

Sample	Formation	Thin Section	Lithology description	Depth
LV44	Hot Spring member	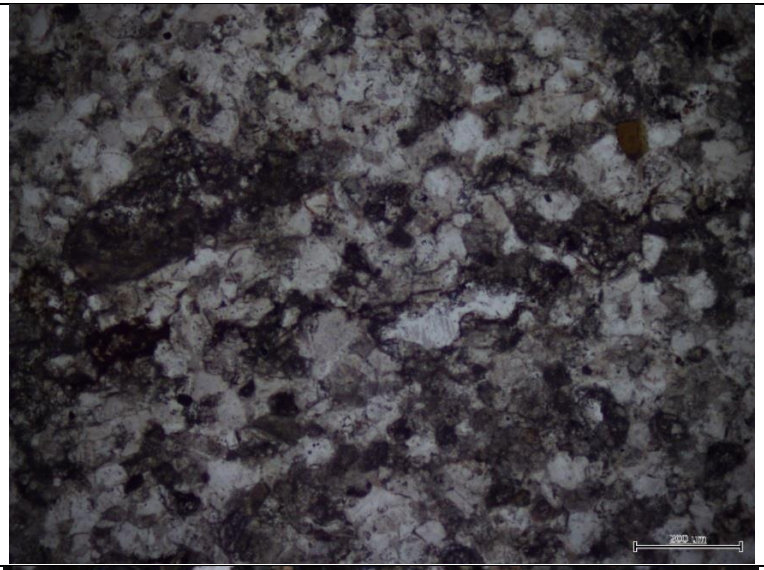 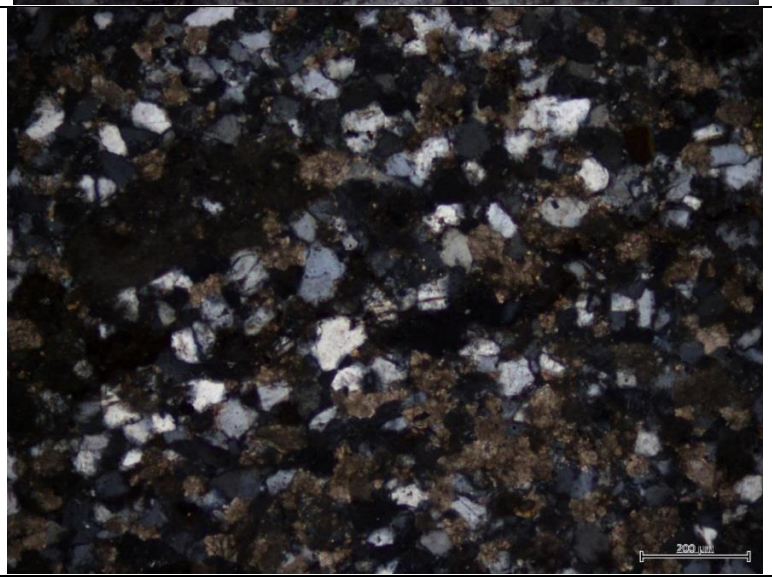		289.85

Sample	Formation	Thin Section	Lithology description	Depth
Lv55	Donnegan	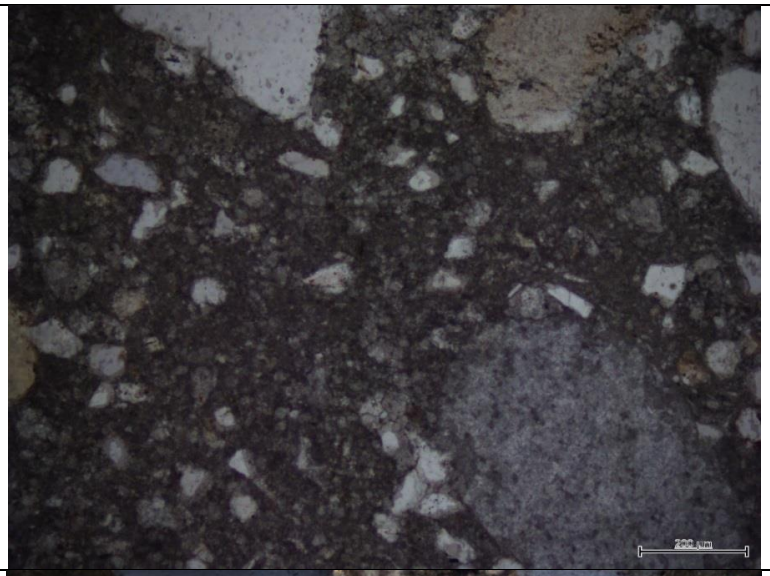 	Black, carbonaceous mudstone with large coarse grained sandstone clasts.	210

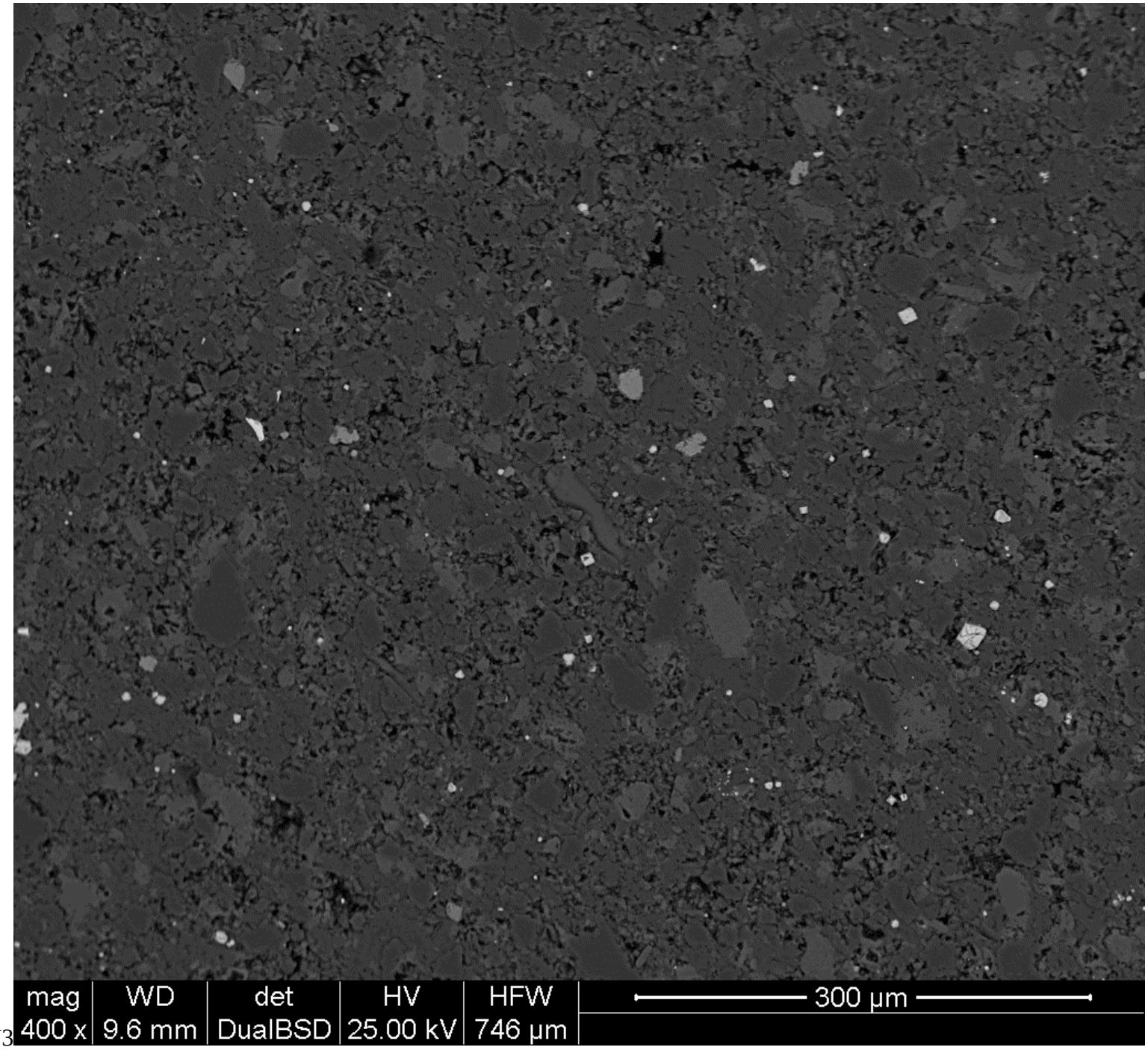

LV3

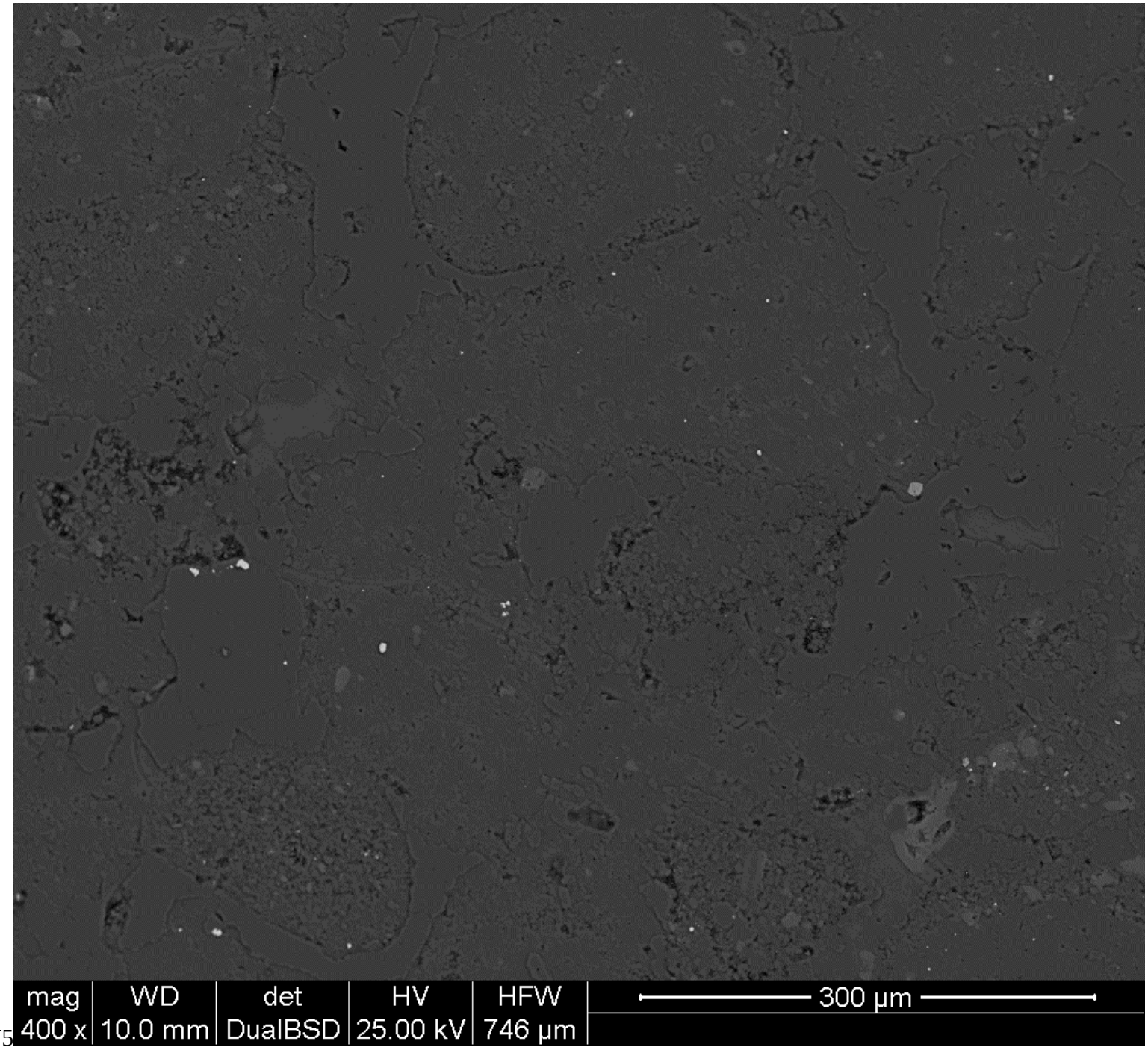

LV5

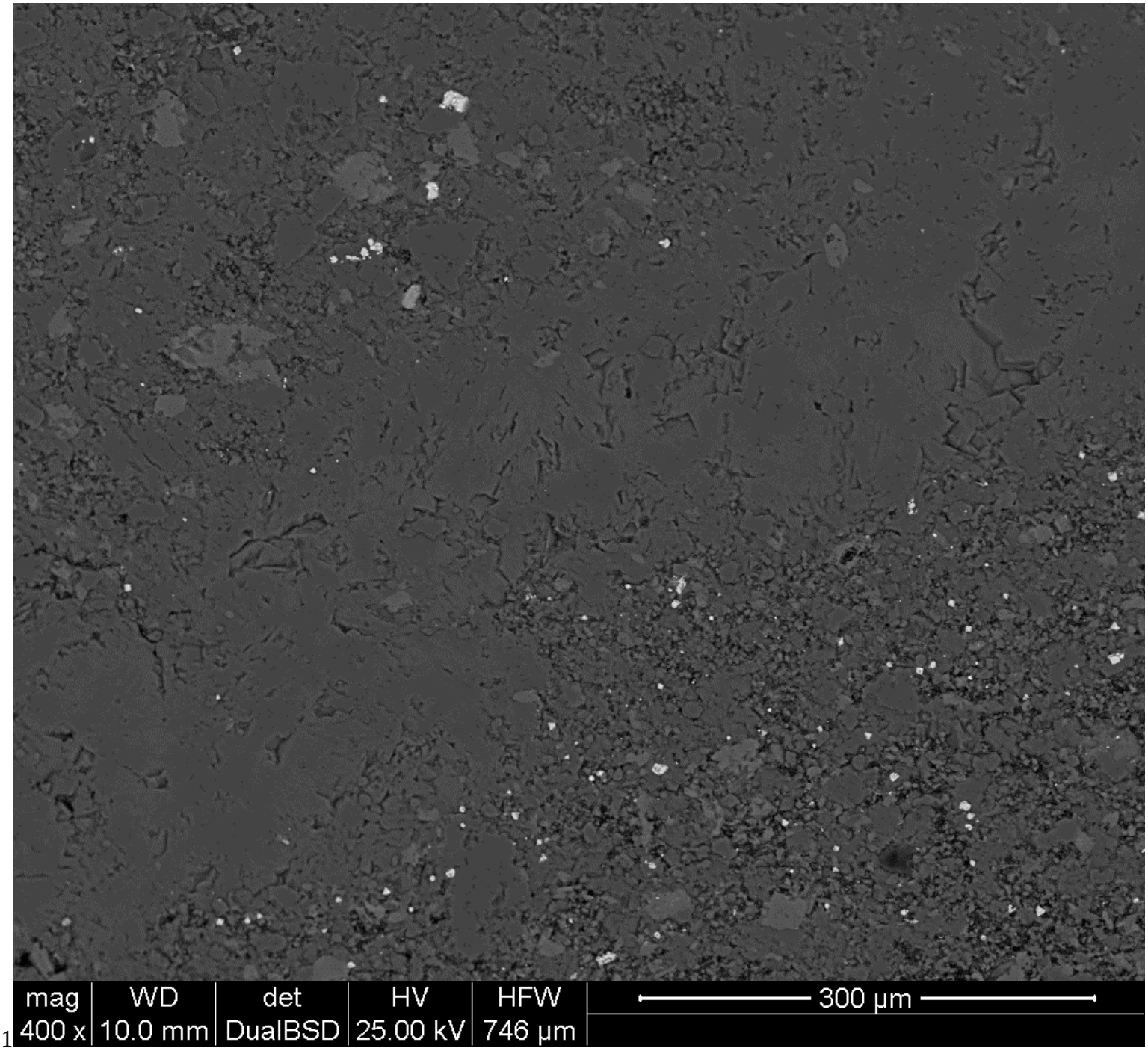

LV11

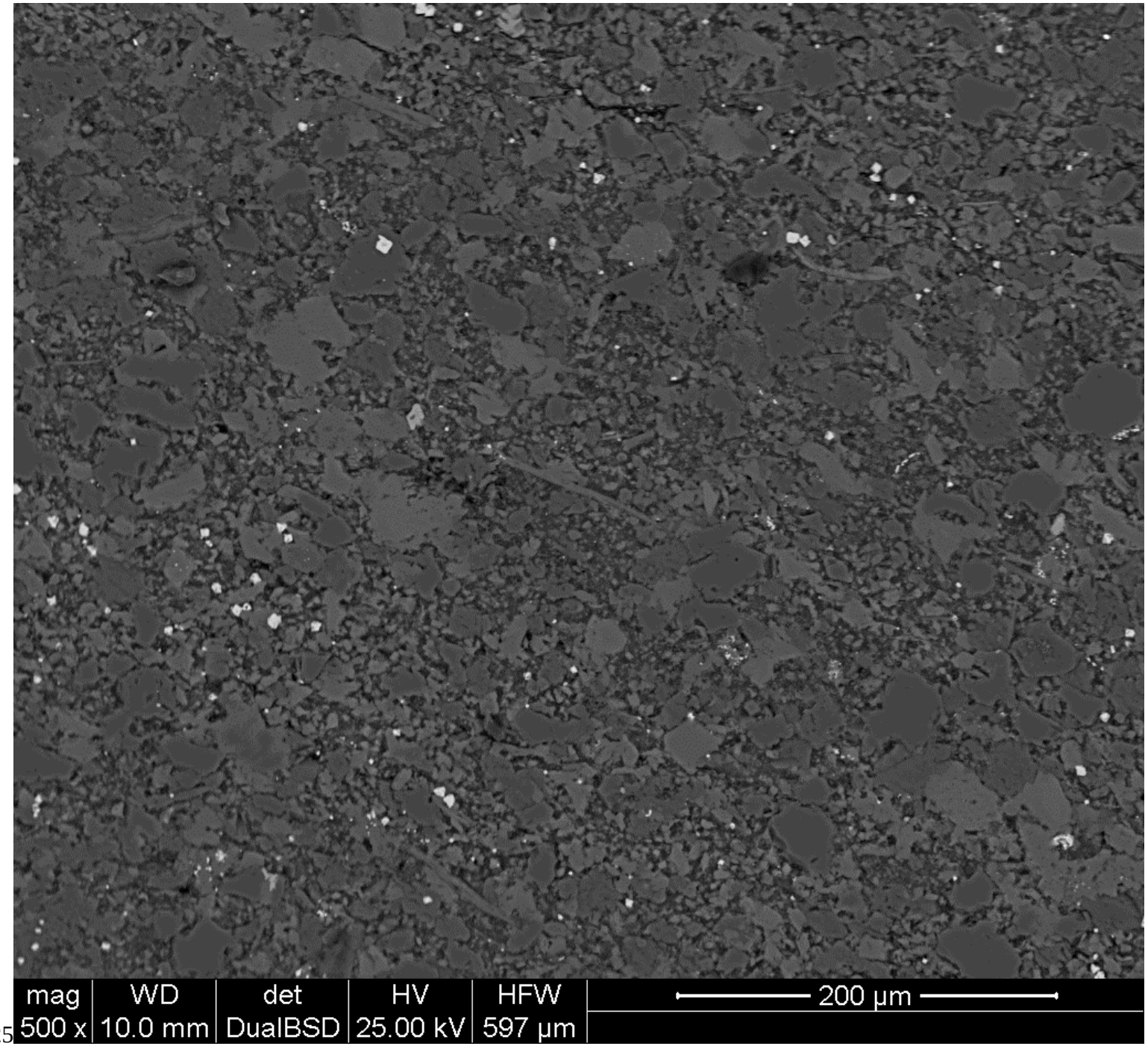
mag
WD
det
HV
HFW
500 x
10.0 mm
DualBSD
25.00 kV
597 µm
200 µm
LV25

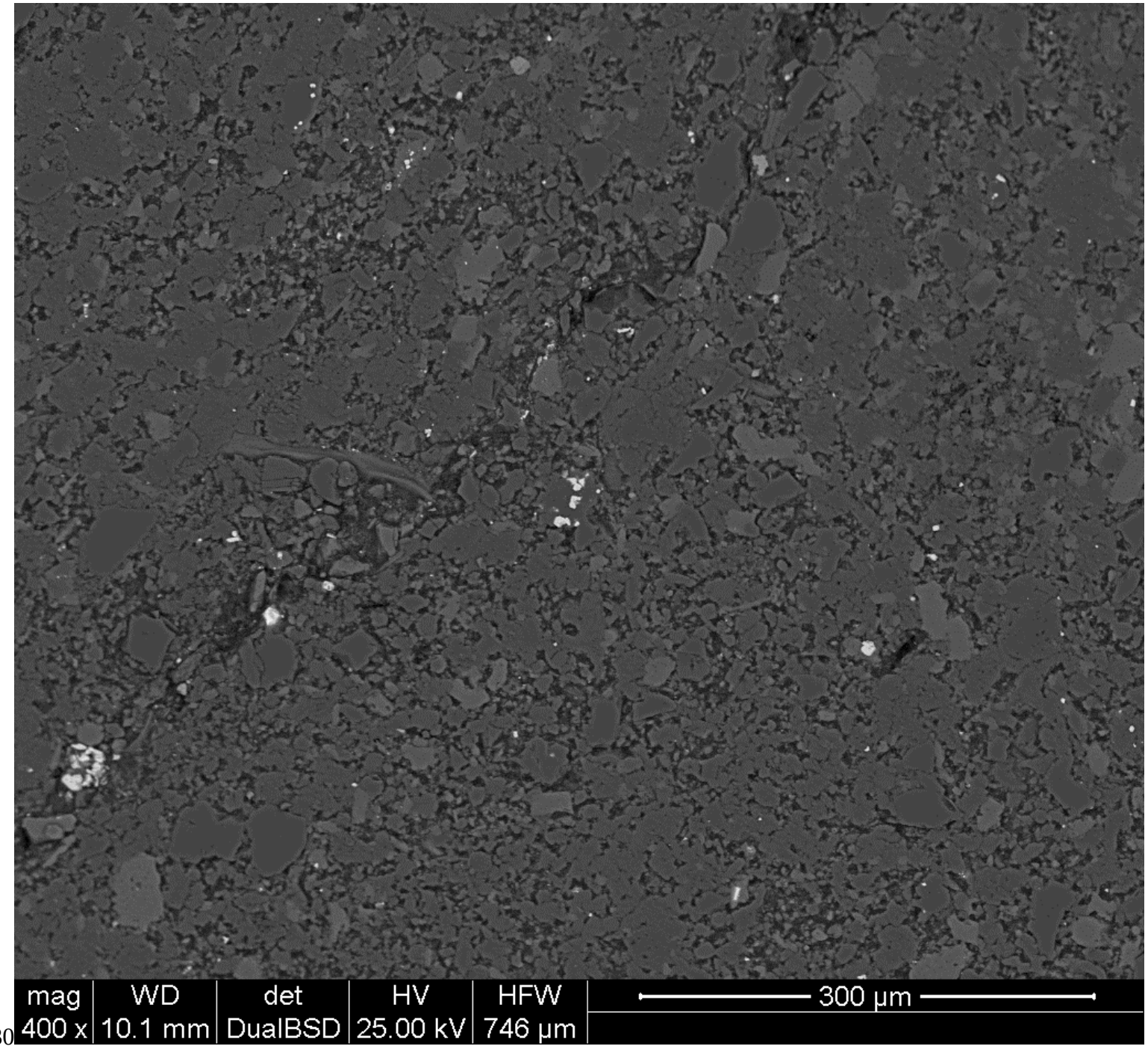

LV30

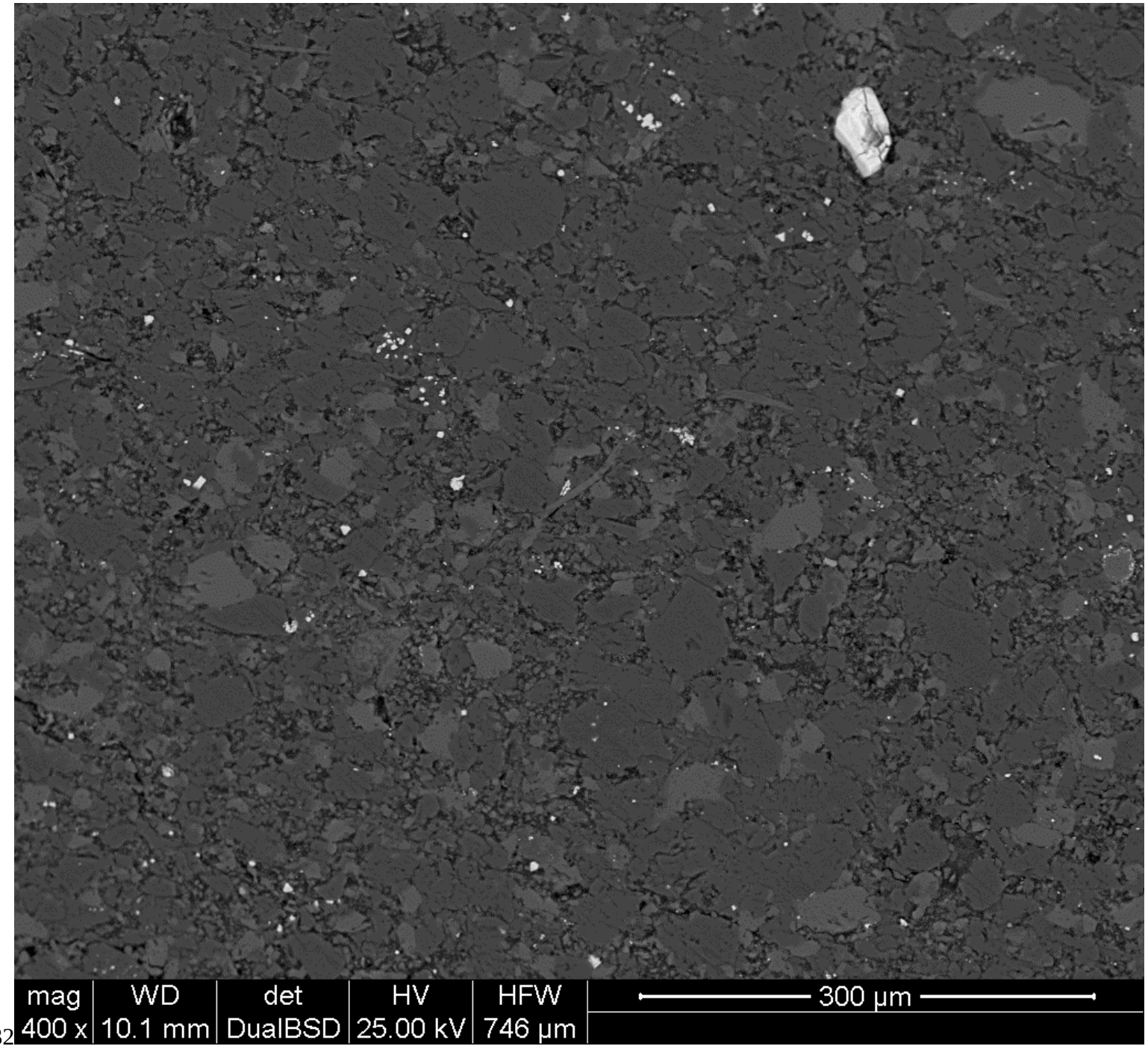
mag
WD
det
HV
HFW
300 µm
400 x
10.1 mm
DualBSD
25.00 kV
746 µm
LV32

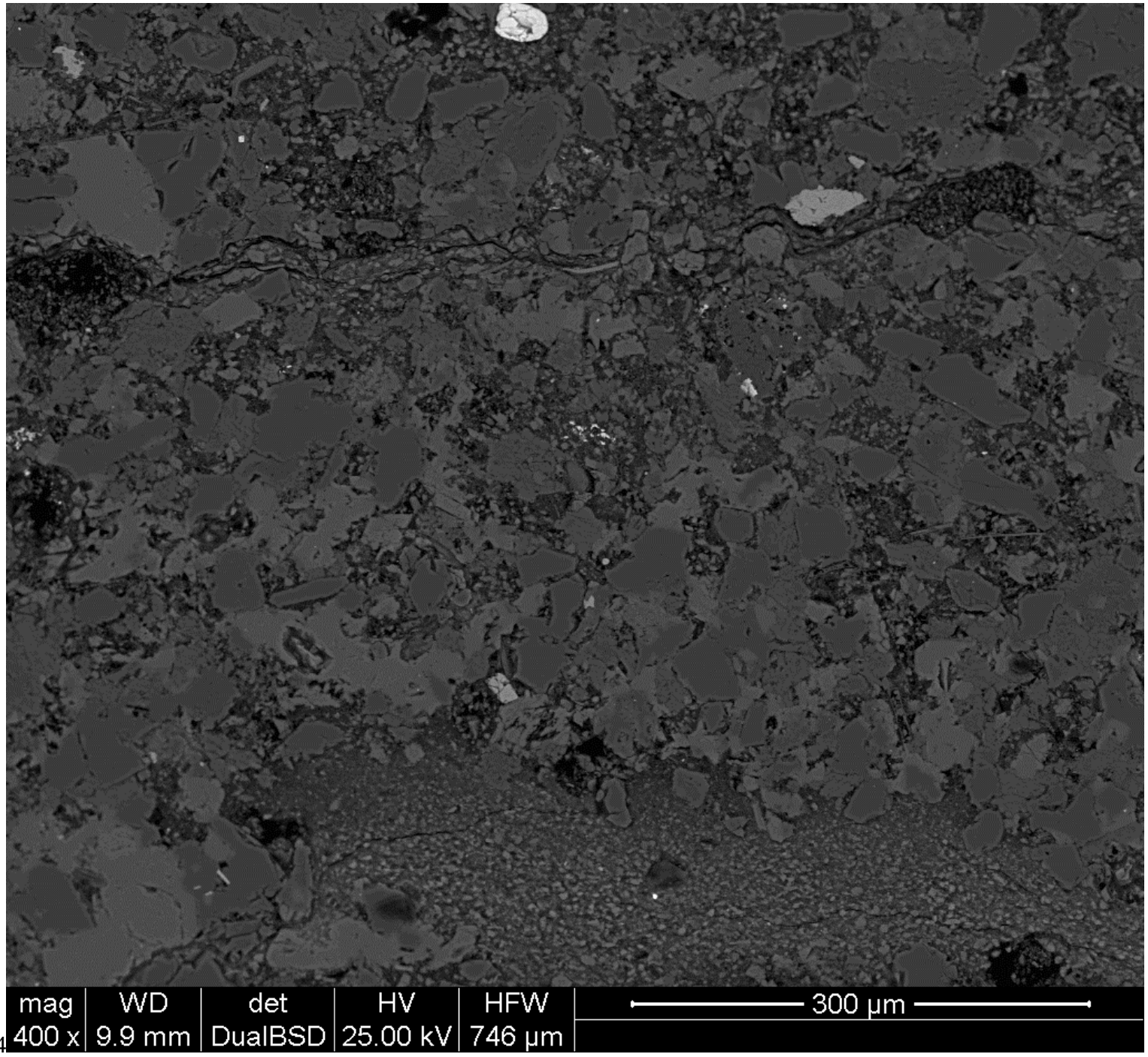

LV44

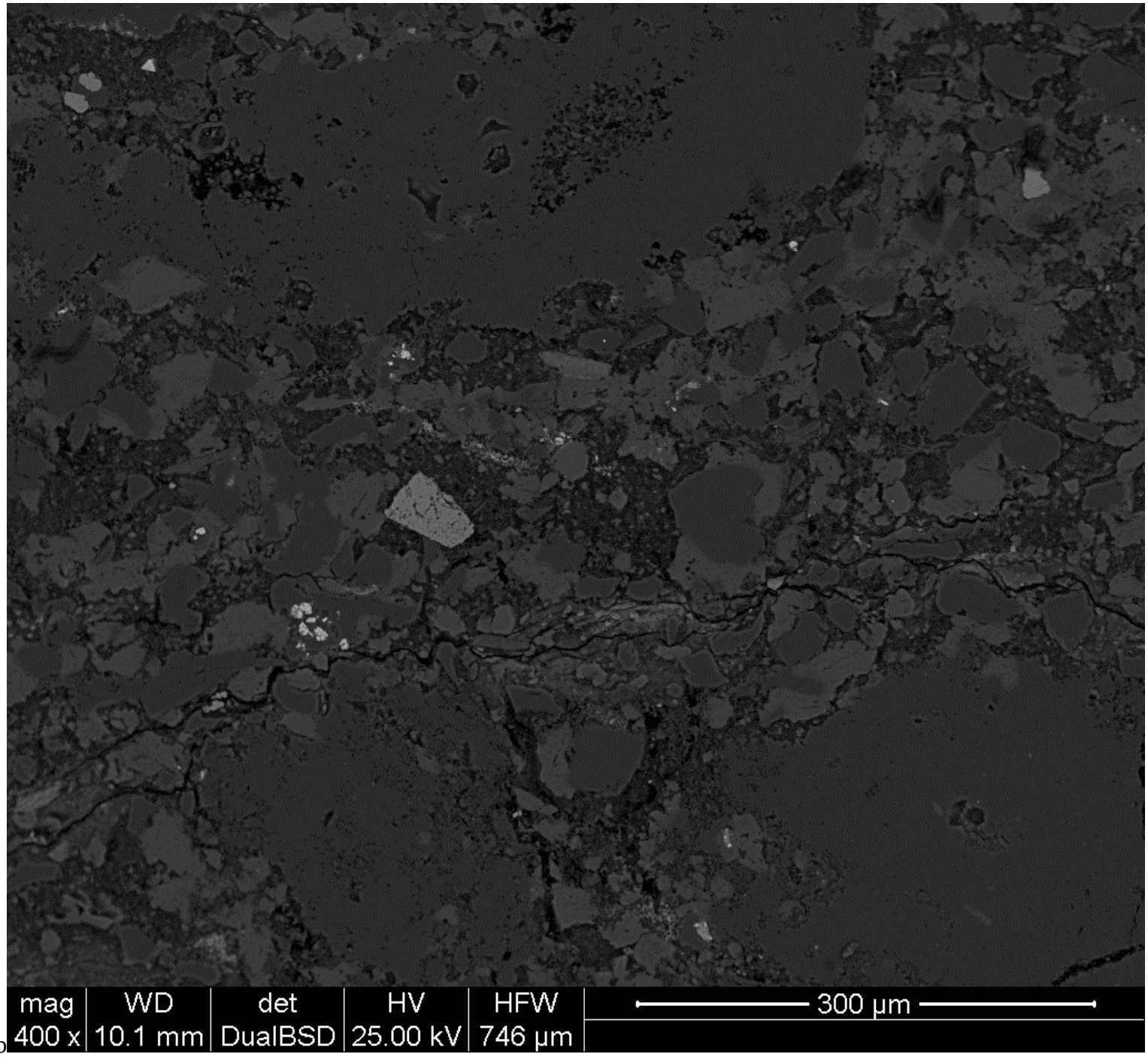

LV46b

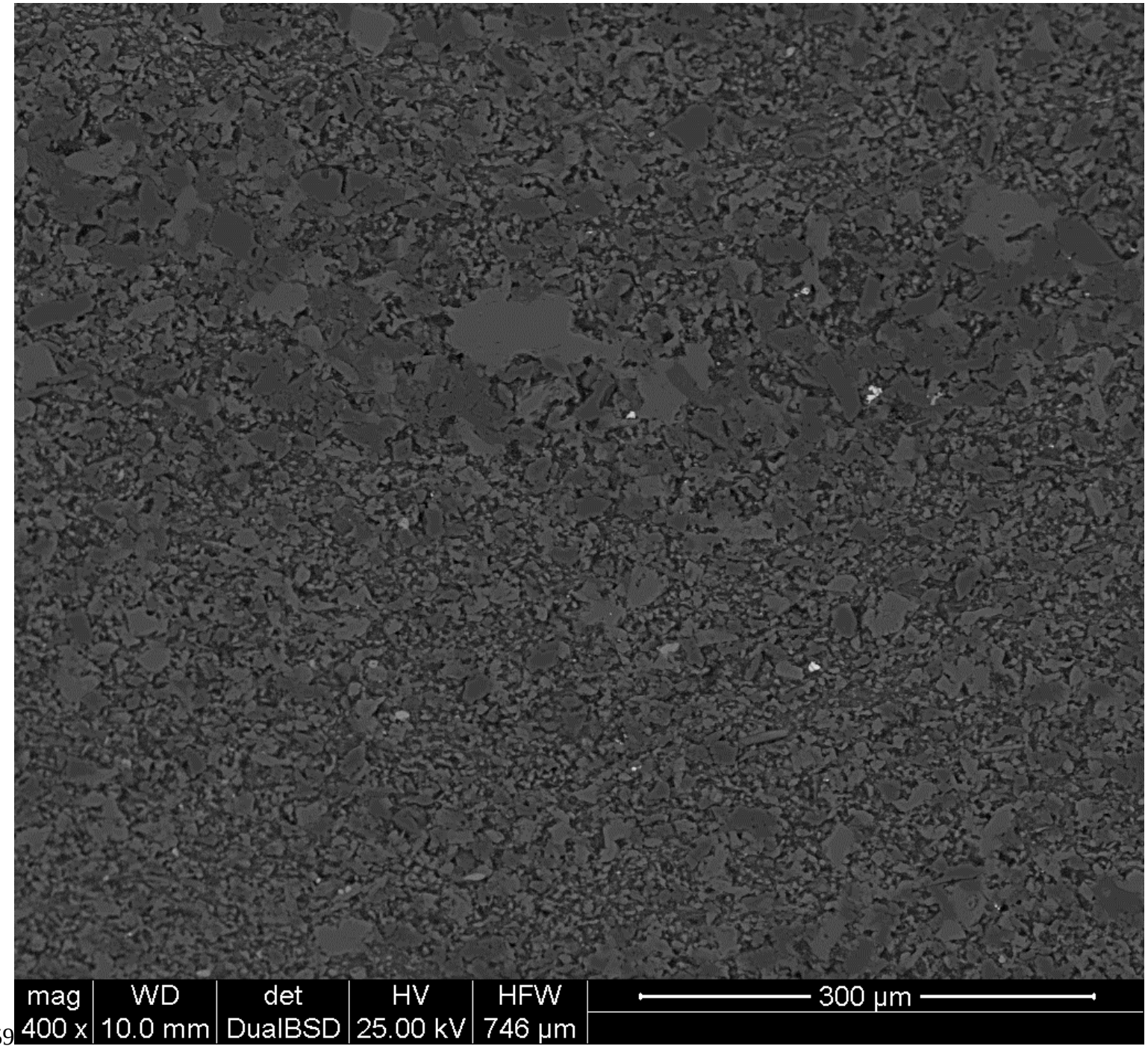

LV59

DOLOMITE PERCENTAGE, CARBON AND OXYGEN ISOTOPE RATIOS

	Depth	$\delta^{13}C$	stdv	$\delta^{18}O$	stdv	% dolomite	% error
Donnegan Member	164.19	-1.80	0.03	-4.95697	0.11	43	3
	164.19	-1.83	0.03	-5.22395	0.29	55	5
	172.3	-1.21	0.05	-4.11677	0.05	63	5
	184.2	-0.97	0.05	-3.91521	0.18	56	4
	184.2	-1.05	0.04	-3.88179	0.20	55	5
	198.2	-0.79	0.11	-4.7931	0.34	57	5
	210	-0.99	0.11	-3.67126	0.16	61	5
	210	-1.08	0.08	-3.80409	0.18	46	4
	219.5	-0.93	0.03	-3.72485	0.02	59	5
	235.4	-1.13	0.02	-5.04642	0.18	43	3
	252.55	-1.05	0.02	-6.01679	0.31	49	4

	Depth	$\delta^{13}C$	stdv	$\delta^{18}O$	stdv	% dolomite	% error
Hot Springs Member	279.35	-1.58	0.16	-5.64243	0.33	24	2
	279.35	-1.54	0.07	-6.27995	0.09	25	2
	289.85	-1.21	0.05	-6.16206	0.18	39	3
	294.3	-1.24	0.05	-6.24324	0.06	51	4
	301.05	-1.42	0.05	-5.95233	0.26	51	4

	Depth	$\delta^{13}C$	stdv	$\delta^{18}O$	stdv	% dolomite	% error
Reward Dolomite	313.43	-0.63	0.05	-5.09563	0.19	66	5
	313.43	-0.59	0.04	-5.01547	0.21	66	5
	318.6	-0.86	0.03	-3.77662	0.21	51	4
	330.4	-0.70	0.05	-7.21133	0.13	50	4
	330.4	-0.69	0.05	-6.55981	0.07	60	5
	341.1	-0.25	0.02	-4.51057	0.13	80	6
	350.9	-0.52	0.11	-6.92351	0.20	46	3
	360.2	-0.50	0.09	-7.62452	0.18	45	3
	360.2	-0.40	0.05	-7.66957	0.27	38	3

	Depth	$\delta^{13}C$	stdv	$\delta^{18}O$	stdv	% dolomite	% error
Barney Creek Formation	369.81	-0.67	0.07	-7.38217	0.11	28	2
	373.85	-0.34	0.01	-6.09104	0.11	70	5
	376.4	-0.50	0.03	-7.01126	0.12	63	5
	380.7	-0.61	0.02	-6.34674	0.08	69	5
	386.9	-0.80	0.04	-7.02316	0.10	75	6
	393.7	-0.91	0.07	-5.76115	0.06	82	6
	393.7	-0.94	0.01	-6.24017	0.15	73	6
	399.5	-0.73	0.08	-6.86628	0.35	61	5
	412.88	-1.02	0.03	-6.98094	0.12	59	4
	412.88	-1.01	0.05	-6.66917	0.14	62	5
	419.66	-1.50	0.04	-6.41431	0.14	62	5
	432.54	-1.48	0.06	-6.30037	0.32	25	2
	445	-1.67	0.02	-6.88796	0.06	76	6
	452.1	-2.08	0.07	-5.62029	0.16	17	2
	463.6	-1.87	0.02	-6.44165	0.08	50	4
	463.6	-1.98	0.04	-5.9878	0.15	57	5
	469.5	-1.51	0.05	-6.79879	0.15	59	4
	490.7	-1.31	0.07	-6.00911	0.19	52	4
	502.5	-2.28	0.05	-7.2805	0.12	15	2
	508.1	-1.78	0.04	-5.42608	0.23	42	3
	515	-1.94	0.06	-6.46991	0.23	68	5

	Depth	$\delta^{13}C$	stdv	$\delta^{18}O$	stdv	% dolomite	% error
Cooley Dolomite	530	-1.18	0.03	-7.25897	0.33	61	5
	534.25	-1.08	0.07	-8.24885	0.06	83	6
	534.25	-1.23	0.11	-7.81974	0.08	44	3
	540.02	-1.02	0.11	-8.18606	0.13	82	6
	543	-0.71	0.04	-8.60288	0.09	79	6
	543	-0.86	0.04	-8.3606	0.10	75	6
	547.61	-0.81	0.02	-8.29015	0.13	73	6

	Depth	$\delta^{13}C$	stdv	$\delta^{18}O$	stdv	% dolomite	% error
Teena Dolomite	553.9	-0.60	0.10	-8.38516	0.09	42	3
	553.9	-0.79	0.08	-8.9781	0.26	39	3
	554.1	-0.73	0.05	-8.30058	0.23	75	6
	565.7	-0.81	0.04	-8.14049	0.21	71	5
	567.5	-0.91	0.06	-8.92403	0.13	50	4
	568.28	-0.59	0.03	-7.91219	0.22	91	7
	568.28	-0.63	0.02	-8.49877	0.27	89	7
	573.16	-0.62	0.03	-7.43771	0.23	94	8

	Depth	$\delta^{13}C$	stdv	$\delta^{18}O$	stdv	% dolomite	% error
Emmerugga Dolomite	592.48	-0.75	0.05	-9.09133	0.06	52	4
	601.7	-0.52	0.05	-7.89705	0.28	79	7
	603.83	-0.55	0.03	-7.32085	0.14	83	7

Strontium Isotopes ratios

Depth	$^{87}Sr/^{86}Sr$	stdv
164.2	0.7257	0.0018
172.3	0.7292	0.0018
198.2	0.7180	0.0019
210.0	0.7246	0.0019
252.6	0.7288	0.0021
294.3	0.7152	0.0018
313.4	0.7154	0.0019
341.1	0.7070	0.0017
373.9	0.7082	0.0020
393.7	0.7152	0.0028
412.9	0.7257	0.0019
419.7	0.7360	0.0020
445.0	0.7221	0.0021
463.6	0.7227	0.0018
490.7	0.7237	0.0020
502.5	0.7337	0.0019
515.0	0.7109	0.0023
534.3	0.7169	0.0016
567.5	0.7094	0.0019
601.7	0.7071	0.0019
603.8	0.7062	0.0024

SOLUTION ICPMS ELEMENTAL CONCENTRATIONS

Formation	Depth (m)	Mg ppb	Al	P	Ca	Cr	Mn	Fe	Cu	Zn	Sr	Ba	In
DM	164.2	256965.2	20077.7	611.1	493405.4	213.99	9355.00	22300.2	35.510	44.561	327.256	264.512	46259.10
	172.3	277979.7	29629.9	717.5	538468.0	66.60	6832.34	33806.5	39.889	94.718	493.516	318.797	46550.20
	198.2	402359.1	43780.3	871.4	761547.2	32.94	8672.18	49305.8	13.368	136.415	967.190	404.059	46931.47
	210.0	232344.9	31463.2	926.7	401490.5	89.10	8276.12	29092.6	7.989	58.432	531.856	302.106	48212.70
	252.6	193753.5	21717.5	903.5	376890.2	41.10	5070.22	23344.4	12.027	17.515	255.492	289.631	51457.88
HSF	294.3	527930.3	6619.2	649.6	1126904.5	26.46	14362.74	30018.4	19.418	64.401	252.405	191.444	47363.00
RD	313.4	356133.1	12600.8	711.0	781564.7	13.79	11713.04	38445.3	4.313	17.519	496.356	206.897	52140.39
	341.1	540907.8	3190.8	546.2	1176807.8	62.02	18552.15	41920.5	12.873	28.329	982.716	111.337	50624.86
BCF	373.9	349916.0	7316.2	636.5	740249.2	54.84	8541.57	33618.3	3.814	35.838	489.688	244.112	53355.08
	393.7	217083.2	9553.4	744.4	426760.8	11.49	8864.02	34345.7	26.760	10.609	368.791	205.737	56698.55
	412.9	349960.6	9899.1	1668.2	763417.1	29.53	10185.85	36672.7	12.564	18.193	229.623	321.092	51715.38
	419.7	339012.0	14008.7	4050.7	756163.5	31.94	8868.45	46740.4	26.866	23.952	219.599	408.220	52615.70
	445.0	426699.3	11963.3	1048.5	935447.9	40.84	12308.98	63920.9	25.031	49.316	295.557	319.303	54342.38
	463.6	298587.2	11816.1	1820.9	664778.9	29.85	16505.46	39495.7	23.999	44.630	366.798	363.828	57173.96
	490.7	265561.9	11714.4	3226.0	580584.1	40.61	12670.62	36271.8	15.266	46.589	304.376	348.604	58402.31
	502.5	79344.9	13174.1	2041.4	161347.2	18.12	2413.61	27363.1	11.715	61.780	207.428	394.958	58733.83
	515.0	353492.4	8852.8	1050.3	772521.4	34.69	6486.70	45281.9	10.915	134.133	649.514	235.617	61171.26
CD	534.3	535431.2	9198.5	889.2	1110368.9	69.33	10061.74	41802.6	8.076	15.709	196.990	173.301	55359.88
TD	567.5	578918.2	5440.3	1294.4	1208953.0	116.26	10187.41	45379.6	15.417	59.131	298.276	143.373	59634.18
EM	601.7	653795.3	4019.7	1345.5	1339827.5	75.17	5842.62	32742.4	15.706	29.047	433.485	111.892	61040.72
	603.8	605457.2	1812.5	602.2	1214758.0	25.19	4537.26	21529.6	8.417	34.471	376.026	51.926	63478.22

Depth vs concentration of elements throughout LV09001 measured in PPB. Different formations are indicated with different colours. An internal standard of indium was mixed online with the samples to compensate for matrix effects. DM-Donnegan Member, HSF-Hot Springs Formation, RD- Reward Dolomite, BCF-Barney Creek Formation, CD-Cooley Dolomite, TD-Teena Dolomite, EM-Emmerugga Dolomite.